Journal of Advances in Modeling Earth Systems

Supporting Information for

Characterizing the impacts of turbulence closures on real hurricane forecasts: a comprehensive joint assessment of grid resolution, horizontal turbulence models, and horizontal mixing length

Oussama Romdhani[1], Jun A. Zhang[2,3], and Mostafa Momen[1]

[1]Department of Civil and Environmental Engineering, University of Houston, Houston, Texas, USA

[2]NOAA/AOML/Hurricane Research Division, Miami, Florida

[3]Cooperative Institute for Marine and Atmospheric Studies, University of Miami, Miami, Florida

Contents of this file

Introduction

The supporting information provides additional data and analysis that were not presented in the main manuscript. This includes numerical methodology, details of our error calculations, and other complementary data and analysis to support the discussion in the paper.

Text S1. Numerical Methodology

Governing Equations

The Advanced Research WRF (ARW) version 4.1 is adopted in this study to simulate the considered hurricane cases. The ARW code integrates a set of fully compressible, non-hydrostatic Euler equations at each time step. The dynamics solver of the ARW is built upon an Arakawa C-grid staggering horizontally and terrain-following hydrostatic pressure coordinates vertically (Skamarock et al., 2019). To facilitate map projections and curvature terms, anisotropic transformations from computational to physical space were introduced with the release of the ARW V3. In the ARW's computational space – Δx and Δy, the grid size in the meridional and zonal direction – are constant. Hence, to fit the orthogonal projections to the sphere, map scale factors (m_x, m_y), defined as the ratio of the computational distance to the corresponding distance on the earth's surface, are used to adjust the governing equations:

$$m_x = \frac{\Delta x}{Distance\ on\ the\ earth}, \qquad m_y = \frac{\Delta y}{Distance\ on\ the\ earth}. \tag{1}$$

The ARW implements the transformations by rescaling the variables in the momentum and temperature equations as:

$$U = \frac{\mu_d u}{m_y}, \qquad V = \frac{\mu_d v}{m_x}, \qquad W = \frac{\mu_d w}{m_y}, \qquad \Omega = \frac{\mu_d \dot{\eta}}{m_y}, \qquad \Theta_m = \mu_d \theta_m, \tag{2}$$

where u, v, w, are respectively the longitudinal, latitudinal and vertical velocities, μ_d represents the mass of the dry air in the vertical column, η the terrain-following hydrostatic-pressure vertical coordinate, $\dot{\eta}$ the contravariant vertical velocity, Ω the vertical velocity in terms of η coordinate, and θ_m denotes the moist potential temperature (Skamarock et al., 2019). Using the defined variables, the governing equations in the ARW can be written as

Conservation of Mass:

$$\frac{\partial \mu_d}{\partial t} + m_x m_y \left[\frac{\partial U}{\partial x} + \frac{\partial V}{\partial y} \right] + m_y \frac{\partial \Omega}{\partial \eta} = 0. \tag{3}$$

Conservation of Momentum:

$$\frac{\partial U_i}{\partial t} + m_i \left[\frac{\partial \left(U u_i \right)}{\partial x} + \frac{\partial \left(V u_i \right)}{\partial y} \right] + \frac{m_i}{m_x} \frac{\partial \left(\Omega u_i \right)}{\partial \eta} + m_i^r \left[\mu_d \alpha \frac{\partial p}{\partial x_i} + \frac{\alpha}{\alpha_d} \frac{\partial p}{\partial \eta} \frac{\partial \phi}{\partial x_i} \right] - \frac{\delta_{i3} g}{m_y} \left[\frac{\alpha}{\alpha_d} \frac{\partial p}{\partial x_i} - \mu_d \right] = F_i, \tag{4}$$

Conservation of Energy (Potential Temperature Form):

$$\frac{\partial \Theta_m}{\partial t} + m_x m_y \left[\frac{\partial \left(U\theta_m \right)}{\partial x} + \frac{\partial \left(V\theta_m \right)}{\partial y} \right] + m_y \frac{\partial \left(\Omega\theta_m \right)}{\partial \eta} = F_{\Theta_m}, \tag{5}$$

where $x_i = (x, y, \eta)$ is the position vector, $u_i = (u_1, u_2, u_3) = (u, v, w)$ the velocity vector, $U_i = (U_1, U_2, U_3) = (U, V, W)$ the redefined velocity vector in Equation 2, p is the full pressure (water vapor and dry air), α_d the inverse density of dry air, α the inverse density of full parcel of air, g the gravitational acceleration, δ_{ij} the Kronecker delta, $m_i \equiv \left(m_x, m_y, m_x \right)$ denotes a defined map scaling vector, and $m_i^r \equiv \left(m_x/m_y , m_y/m_x , 0 \right)$. The right-hand side terms $F_i = (F_U, F_V, U_W)$ and F_{Θ_m} represent forcing terms arising from model physics, turbulent mixing, spherical projections, and the earth's rotation.

The ARW solver models the vertical turbulent fluxes using the planetary boundary layer (PBL) schemes (Skamarock et al., 2019). The Yonsei University (YSU) PBL scheme (S. Hong, 2010; S. Y. Hong et al., 2006) is a non-local turbulence closure that is employed in this study. YSU has been recommended by the ARW users guide for TC simulations (Wei et al., 2019), and has been extensively used in the ARW hurricane simulations (Cavallo et al., 2013; Davis et al., 2008; Hu et al., 2010; Mooney et al., 2019). Furthermore, it outperforms some local closure PBL schemes in terms of simulating real hurricanes intensities [preliminary results – not shown – and (Nolan et al., 2009)]. In this study, the PBL scheme handles all vertical diffusion calculations in the simulations. The above equations coupled with the scalar conservation equations, the geopotential equation and the equation of state constitute the set of equations solved by the ARW code.

WRF's Surface Fluxes

The ARW model employs three formulations to model the surface fluxes: One formulation for regular weather prediction based on the PBL scheme (Skamarock et al., 2019) and two formulations specifically designed for TCs. One of these TC formulations is based on Donelan et al. (2004), and the other one is a modification of the Donelan parameterization using Garratt's formulation (Garratt, 1994). In the current study, Donelan-Garratt's formulation is used for TC simulations due to its superior performance according to the NCAR's real-time hurricane runs in 2012 (NCAR, 2019). The parameterization used for calculating the surface momentum for all cases is

$$\tau = -\varrho C_D U_L^2, \tag{6}$$

where τ is the surface momentum and U_L is the wind speed. The subscript *"L"* denotes the lowest level. C_D is the dimensionless exchange coefficient for the momentum (drag coefficient). This parameter is defined as

$$C_D = \frac{\kappa^2}{\ln\left(\frac{z_{ref}}{z_0}\right)^2}, \tag{7}$$

where κ is the von Karman constant equal to 0.4, z_{ref} is the lowest level, and z_0 is the momentum roughness length.

Determining the exact drag coefficient for TCs is an open field of research (Jarosz et al., 2007; Powell et al., 2003; Soloviev et al., 2014). In Donelan-Garratt's formulation, the momentum roughness length (z_0) is based on Donelan's parameterization, which uses recent discoveries from field observations and laboratory experiments, indicating that C_D reaches its maximum of 0.003 for TCs with wind speeds ~35 m/s and then stops increasing with an increase in the wind speed (Black et al., 2007; Davis et al., 2008). Therefore, Donelan's momentum roughness length in the code is calculated as

$$z_0 = max\left[1.27\times10^{-7}, min\left[z_w z_2 + \left(1-z_w\right)z_1, 2.87\times10^{-3}\right]\right] \tag{8}$$

$$z_w = min\left(1, \left[\frac{u_*}{1.06}\right]^{0.3}\right) \tag{9}$$

$$z_1 = 0.011\frac{u_*^2}{g} + 1.59\times10^{-5}, \tag{10}$$

$$z_2 = \frac{10}{exp\left(9.5u_*^{-1/3}\right)} + \frac{1.65\times10^{-6}}{max\left(u_*, 0.01\right)}, \tag{11}$$

where u_* represents the friction velocity.

WRF Configuration, Initial and Boundary Conditions

The time integration in the ARW solver is evolved by Runge-Kutta 2nd (RK2) and 3rd (RK3) order time-split integration algorithms (Wicker & Skamarock, 2002). A smaller time step is implemented for acoustic and gravity wave modes and the RK3 scheme is used to integrate momentum and continuity equations. The time step (Δt) in the simulations is fixed according to the following

$$\Delta t = \frac{CFL\Delta x}{U_{ref}}, \tag{12}$$

where Δx is the grid size, CFL refers to Courant-Friedrichs-Lewy number that is set to 0.2 here, and U_{ref} denotes the reference velocity, which is set to 50 m/s here (approximately the average

wind speed of major hurricanes). For instance, for a grid size of 2 km, Δt = 4 s is used, and for a 4 km grid size Δt = 8 s.

The initial and boundary conditions of the simulations were provided by the National Centers for Environmental Prediction's (NCEP) final (FNL) operational global analysis and forecast data. NCEP provided such data every six hours on a 0.25º × 0.25º resolution for both Irma and Maria, and 1º × 1º for Katrina and Gustav.

In the present paper, all WRF experiments were initialized based on the National Centers for Environmental Prediction (NCEP) final analysis data (FNL). These global analysis and forecast data are the product of the Global Data Assimilation System (GDAS) and were built over continuous observational data from the Global Telecommunications System (GTS) and other resources (NCEP, 2000; NCEP, 2015). The NCEP (FNL) parameters include sea level pressure, surface pressure, *u* and *v* wind velocity components, temperature, sea surface temperature, geopotential height, relative humidity, ice cover, vertical motion, vorticity and ozone (NCEP, 2015; NCEP, 2000). These data are provided, vertically, at 26 mandatory levels from 10 millibars to 1000 millibars (at the surface of the boundary layer, some sigma layers, the tropopause, and few other levels). For hurricanes Irma, Maria and Florence, the initial and boundary conditions were defined every 6 hours with a spatial resolution 0.25º × 0.25º and for Katrina and Gustav a coarser grid of 1º × 1º was utilized with the same frequency.

Text S2. Microphysics and radiation schemes

In the current study, the WRF single-moment 3-class microphysics scheme (S. Y. Hong et al., 2004) was employed for all the simulations. This microphysics scheme includes ice sedimentation and other new ice-phase parametrizations. Additionally, a diagnostic relation based on ice mass content is implemented for ice number (Skamarock et al., 2019). With respect to the computational procedure described by (S.-Y. Hong et al., n.d.), the so called simple-ice scheme (WSM3) predicts three types of moist variables: water vapor, cloud (water/ice) and rain/snow. This scheme assumes cloud water and rain for temperatures exceeding freezing degree and snow and cloud ice for temperatures below freezing degree (Dudhia, 1989).

To account for atmospheric temperature tendencies caused by radiative flux divergence and downward surface longwave and shortwave radiation, we employed the Rapid Radiative Transfer Model (RRTM) for longwave radiation (Mlawer et al., 1997) and the MM5 (Dudhia, 1989) for modeling shortwave radiation. The RRTM is a spectral band scheme and defined using the correlated-*k* method. To represent longwave mechanisms due to ozone, CO_2, water vapor and trace gases it refers to pre-set tables while accounting for cloud optical depth. The MM5 (Dudhia, 1989) on the other hand, employs a simple downward integration of solar flux representing water vapor absorption (Lacis & Hansen, 1974), tunable clear-air scattering and cloud albedo and absorption. It also uses pre-set tables for clouds but does not consider sub-grid cloud fractions.

Text S3. Track and wind speed errors in terms of grid size, turbulence model and mixing length

To examine WRF's hurricane track prediction accuracy, we compared the simulated tracks against the best observed track. Figure S.1 exhibits this comparison for hurricanes Irma, Gustav, Katrina, and Maria (Beven II & Kimberlain, 2009; Cangialosi et al., 2018; Knabb et al., 2006; Pasch et al., 2019). The first column depicts the outputs of NoHorizTurb experiments for various grid resolutions. The second and third columns depict the two turbulence models considered in the present work. Although, the simulations were identically initiated for each hurricane, the simulated tracks started to diverge after few hours of simulation in different grid resolutions.

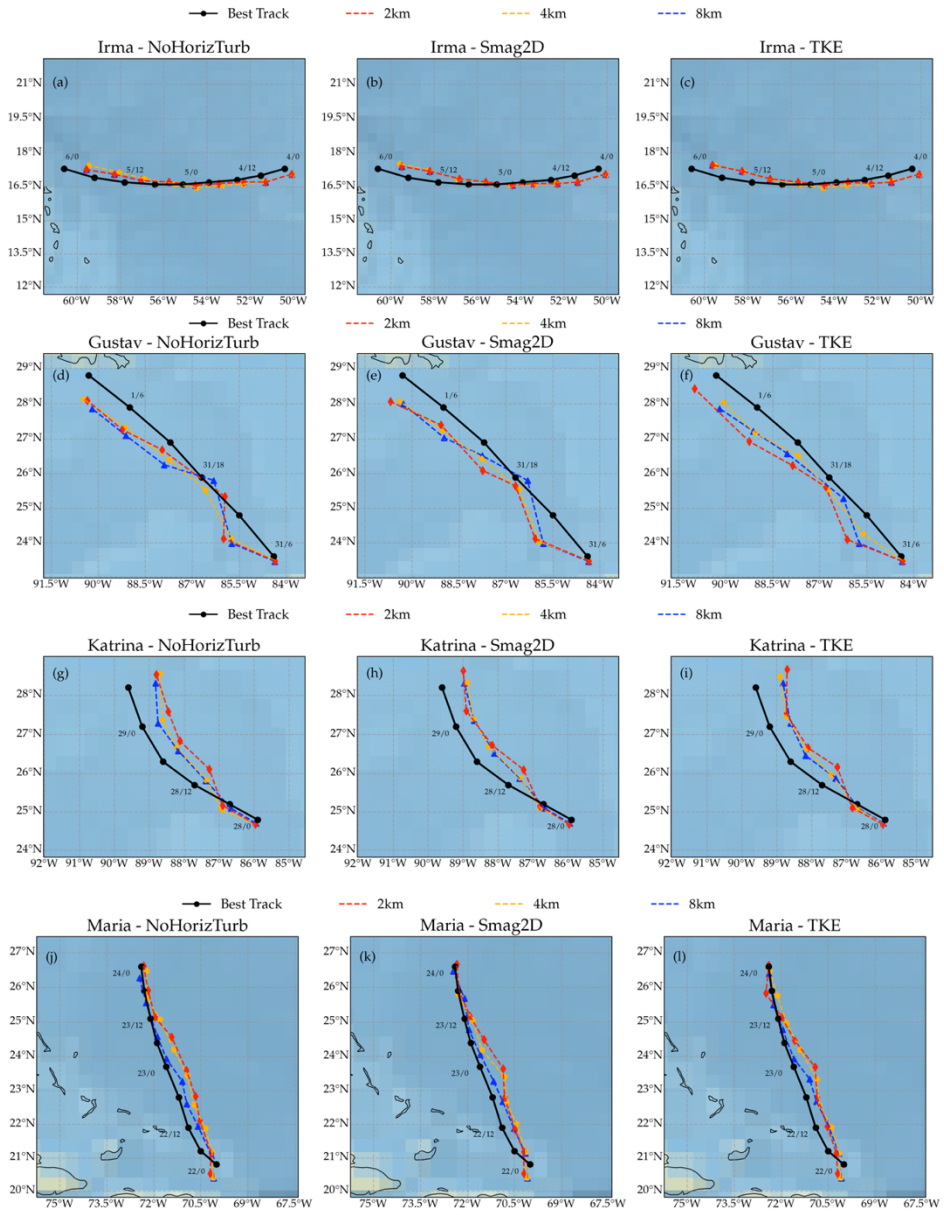

Figure S.1. Best observed track versus the simulated tracks for 2 km, 4 km, 8 km and 16 km grid sizes for hurricanes Irma, Gustav, Katrina, and Maria using the three turbulence models: NoHorizTurb, Smag2D, and TKE.

To elucidate the relationship between WRF's hurricane track predication and the implemented turbulence models, we plotted the track error time series for various grid resolutions in Figure S.2. The track error is calculated by calculating the distance between the simulated track and the best observed track at each time step.

We calculated the MAE_{Track} for each case using the data in figure S.2. Table S1 shows the average track error for each simulation as a function of grid resolution and employed turbulence model. Furthermore, $MAPE_{Intensity}$ for each considered case is shown in this table. In general, WRF tends to perform better over finer grids especially for the wind intensity predictions. Even though, for some cases (e.g., Irma's track) the coarsest grid resolution outperformed the finest, overall, both track error and wind speed error tend to decrease with respect to mesh refinement.

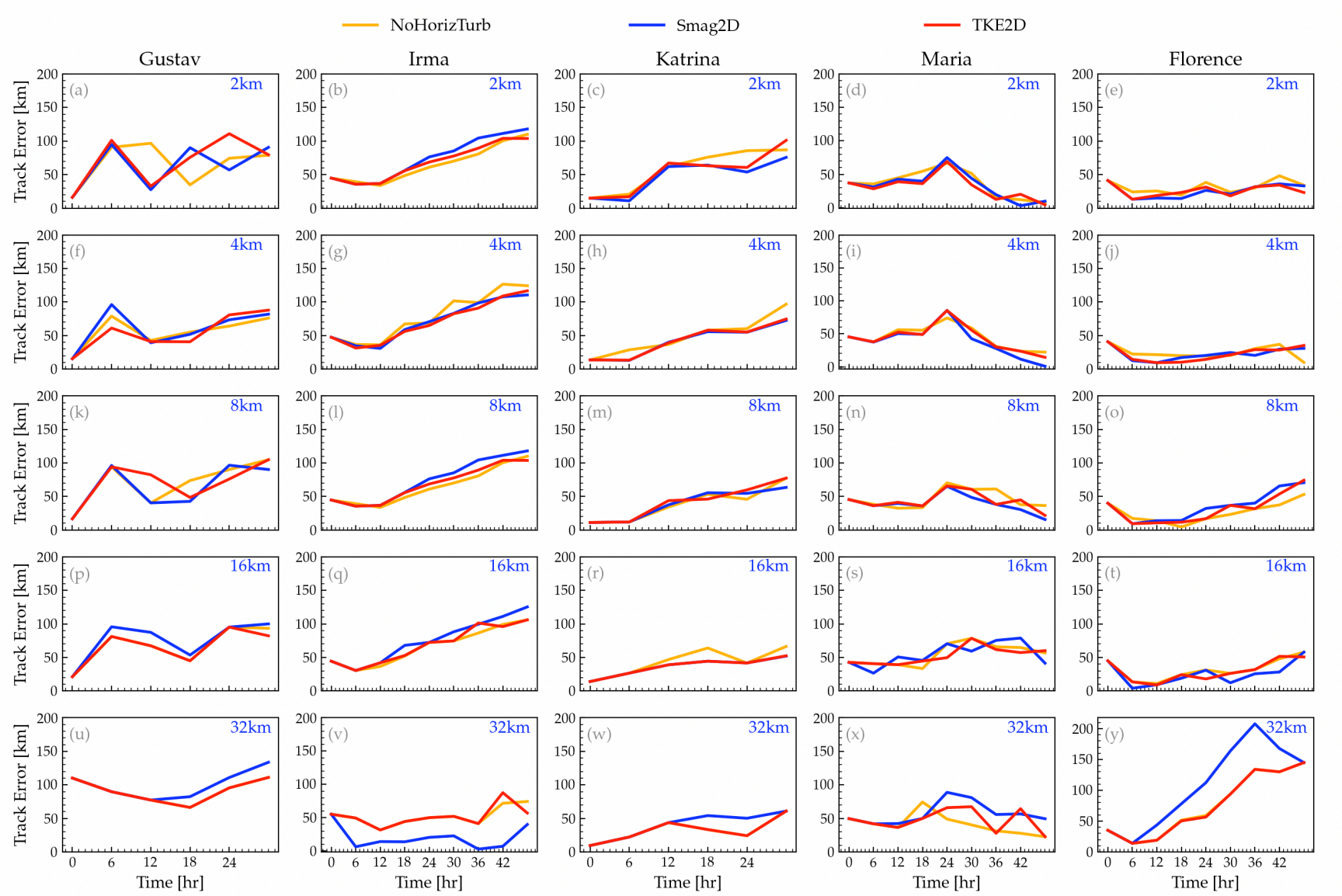

Figure S.2. Track Error vs time for each hurricane, grid length and turbulence model.

Table S1. Average error for each hurricane at different grid resolutions. The table shows two kinds of error: (1) the track error and (2) the wind intensity error, with the red color being the highest average error recorded for different grid resolutions and green the least. The data of this table are used to plot figure 4 of the paper.

		Gustav					Irma					Katrina					Maria					Florence				
		2	4	8	16	32	2	4	8	16	32	2	4	8	16	32	2	4	8	16	32	2	4	8	16	32
MAE_{Track} (km)	NoHorizTurb	65.2	55.4	70	67.3	91.7	65.4	78.7	65.4	66.9	52.2	57.7	49	39	43.3	32.3	36	44.9	46.3	54.7	41.5	31.7	24.6	26.5	32.1	75.7
	Smag2D	62.7	59.7	63.8	75.5	101	74.3	71.4	74.3	75.7	20.3	46.9	41.6	39.1	36.3	40.1	33.5	38.9	39.5	54.6	57.3	25.8	22.9	35.9	25.8	108
	TKE	69.4	54.5	70.5	65.4	91.7	68.5	70.5	68.5	68.9	52.1	54	42.3	41.7	36.4	32.3	31.2	43.7	43.4	52.7	47.4	26.2	22.6	31.7	30.0	75.2
$MAPE_{Intensity}$ (%)	NoHorizTurb	29.8	31.3	29.5	31.7	34.6	18.8	18.9	14.6	19.6	28.9	22	24.1	21.7	28.2	28.7	9.8	12.3	14.4	16.5	25.8	10.8	14.1	14.3	14	22.4
	Smag2D	29.3	29.2	28.4	34.4	37.9	21.6	21.7	26.5	31.6	42.2	19.5	25.1	28.4	30.2	36.4	11.4	18.8	20.3	29.1	34.9	15	19.4	20.4	26.6	37
	TKE	25.7	31.4	29.8	32.4	36.3	22.5	22.7	24.1	26.9	31.5	23.5	27.5	25.9	29.5	31.4	11.6	18.3	16.4	25.8	28.6	10.8	16	17.2	21.8	26.6

To quantify the impact of turbulence models and grid resolution on WRF's hurricane forecasts accuracy, the liner regression between the normalized grid length and the normalized error for each turbulence model was investigated. As Figure S.3 indicates, the obtained ascending trend confirms that the track and intensity errors improve by refining the grid resolution. Furthermore, this figure shows that among the three different turbulence models, NoHorizTurb was the most accurate for wind intensity forecasting while it was not the most efficient scheme for the track prediction.

To assess the effects of the horizontal mixing length scales on the dynamics of the hurricanes, we varied the cL_h from 0.25 to 1.5. Tables S2 and S3 report the average error for each hurricane with different turbulence models at 4km and 32km grid resolutions. The results show that decreasing the mixing length scale from its default value for regular boundary-layer flows increases the model's accuracy for hurricane simulations consistent with Momen et al., (2021) and Zhang (2010). Smag2D was the most sensitive model to cL_h changes. These data are used to depict figure 13 of the paper.

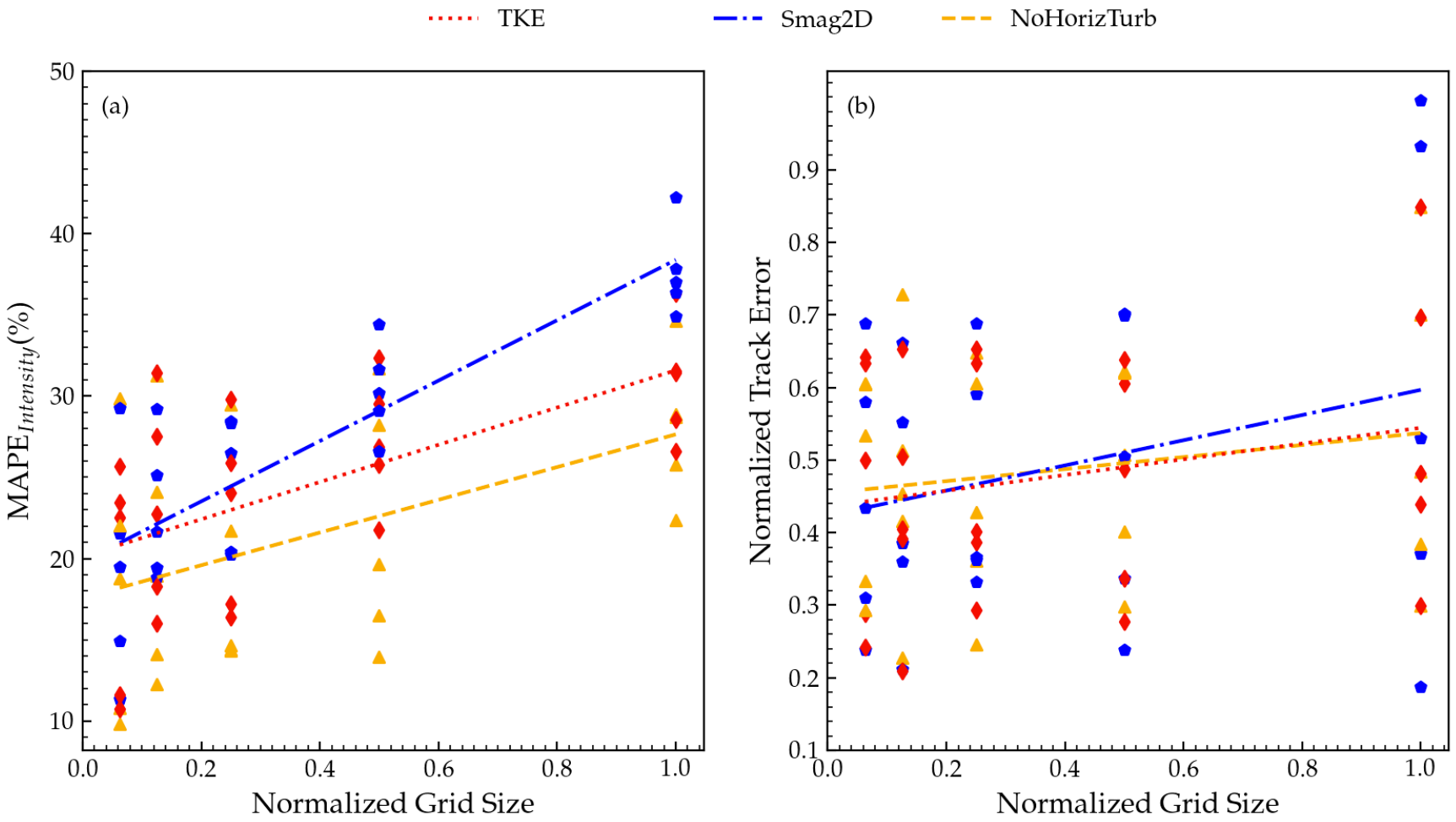

Figure S.3. Linear regression showing the relationship between the normalized grid length and the normalized error for each turbulence model. The data of this figure are used in Table 3 of the paper.

Table S2. Average error for each hurricane with different turbulence models and horizontal mixing lengths at grid resolution of 4 km. The table shows two types of errors: (1) the track error and (2) the wind intensity error with the red color being the highest average error recorded for different grid resolutions and green the least.

		Gustav				Irma				Katrina				Maria				Florence			
		0.25	0.5	1.0	1.5	0.25	0.5	1.0	1.5	0.25	0.5	1.0	1.5	0.25	0.5	1.0	1.5	0.25	0.5	1.0	1.5
MAE_{Track} (km)	NoHoriz Turb			55.4				78.7				49				44.9				24.6	
	Smag2D	58.3	51.1	59.7	66.6	76.8	75.9	71.4	68.3	43.4	39.2	41.6	38.5	39.4	44.6	38.9	42.6	24.9	22.6	22.9	33.2
	TKE	57.3	59.9	54.5	61	80.5	73	70.5	70.7	43.2	51.3	42.3	43.3	43.9	45.5	43.7	45.3	22.6	25.3	22.6	28.1
$MAPE_{Intensity}$ (%)	NoHoriz Turb			31.3				18.4				24.1				12.3				14.1	
	Smag2D	28.4	31.6	29.2	29.7	17.7	18.9	21.7	24.8	26.6	24.8	25.1	29.1	13	15.5	18.8	22	11.9	13.9	19.4	21.3
	TKE	28.4	29.1	31.4	33	20.4	19.1	22.7	23.8	25.5	27.5	27.5	28.5	11.8	12.4	18.3	17.6	14.3	14.5	16	18.8

Table S3. Average error for each hurricane with different turbulence models and horizontal mixing lengths at grid resolution of 32 km similar to Table S.2.

		Gustav				Irma				Katrina				Maria				Florence			
		0.25	0.5	1.0	1.5	0.25	0.5	1.0	1.5	0.25	0.5	1.0	1.5	0.25	0.5	1.0	1.5	0.25	0.5	1.0	1.5
MAE_{Track} (km)	NoHoriz Turb			91.7				52.2				32.3				41.5				75.7	
	Smag2D	91.7	91.7	101	96.0	52.1	48	20.3	30	32.3	36.6	40.1	44.7	42.5	50.2	57.3	74.1	78.6	83.7	107	120
	TKE	91.7	91.7	91.7	91.7	52.2	54	52.1	50.9	32.3	32.3	32.3	32.3	36.1	42.2	47.4	55.3	75.4	75.7	75.3	81.1
$MAPE_{Intensity}$ (%)	NoHoriz Turb			34.6				28.5				28.7				25.8				22.4	
	Smag2D	35.8	36.2	37.9	41.7	30.6	33.7	42.2	49.2	28.9	31.9	36.4	43.2	26.2	29.2	34.9	40.2	23.9	28.8	37	44.4
	TKE	35	35.7	36.3	37	29.8	30.4	31.5	35	28.8	28.8	31.4	32.5	25.7	26.6	28.6	31.1	22.6	24	26.6	30.3

Text S4. Smagorinsky 3D turbulence closure:

The Smagorinsky 3D closure implements horizontal and vertical eddy viscosities as given by equations 13.1 and 13.2

$$K_h = C_s^2 l_h^2 \, max\left[0., \left(D^2 - P_r^{-1} N^2\right)^{1/2}\right], \tag{13.1}$$

$$K_v = C_s^2 l_v^2 \, max\left[0., \left(D^2 - P_r^{-1} N^2\right)^{1/2}\right], \tag{13.2}$$

where

$$D^2 = \frac{1}{2}\left[D_{11}^2 + D_{22}^2 + D_{33}^2\right] + \left(\overline{D_{12}}^{xy}\right)^2 + \left(\overline{D_{13}}^{x\eta}\right)^2 + \left(\overline{D_{23}}^{y\eta}\right)^2. \tag{33.3}$$

WRF's user guide recommends the implementation of the 3D Smagorinsky model for a grid resolution of 2 km (Wei et al., 2019). Thus, the selected hurricanes were simulated using this resolution and the average $Mape_{Intensity}$ and MAE_{Track} values are given in comparison to other models in figure S.4.

The results show that, in terms of intensity predictions, Smag3D yields the lowest MAPE value of ~16%. However, Smag2D, TKE and NoHorizTurb outperform Smag3D in terms of track forecasts. We note that the vertical diffusion in the three considered models is handled by the YSU PBL scheme.

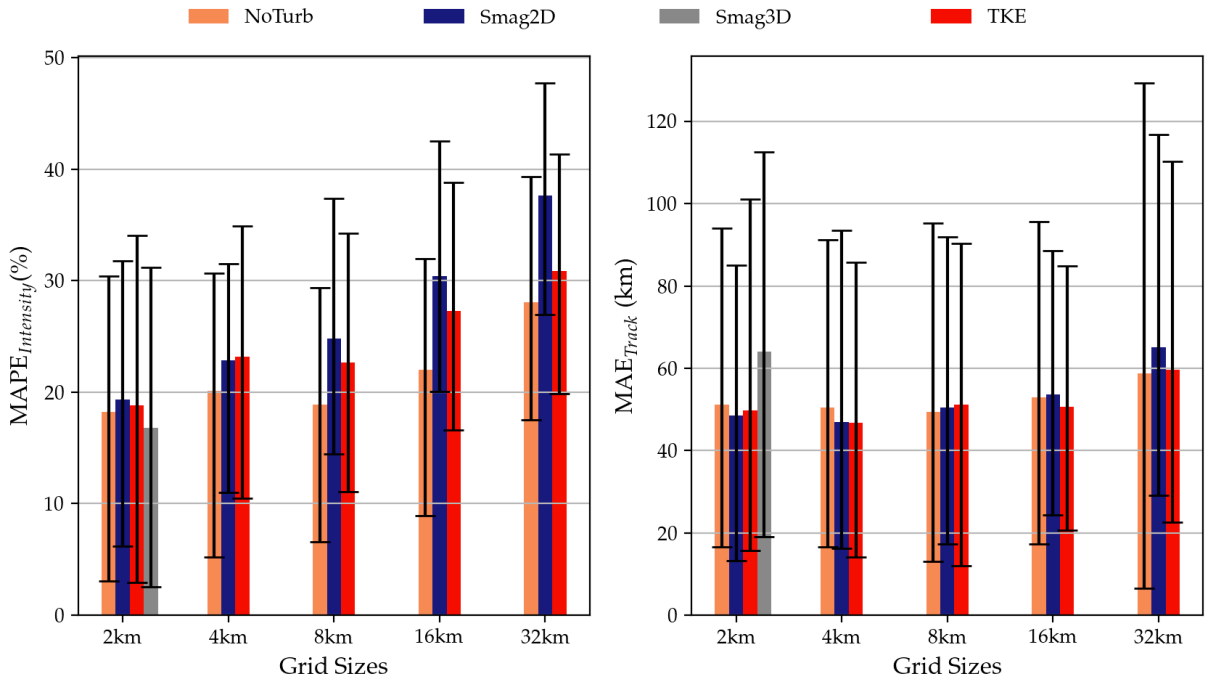

Figure S.4. Average error of all hurricanes in terms of grid sizes and default turbulence models. The solid black lines represent the 10th and 90th percentiles error bars.

Text S5. Wind speed contour maps of Hurricanes Irma, Katrina, Gustav and Maria for changing the horizontal mixing length

Figures S.4.1 and S.4.2 show the wind intensity contour maps at 500 meters of altitude and the sea level pressure isolines for each hurricane with Smag2D and TKE turbulence models respectively for 32km and 4km grid resolutions. Both figures indicate that decreasing the cL_h by a factor of 1/4 yields an increase of the average and maximum wind intensity at 500 meters above the sea level (see the shift from bluish and yellowish contour map for cL_h =1.5 to reddish contour map for cL_h =0.25) and a decrease of the minimum sea level pressure at the center of the hurricane. For the TKE turbulence model simulations, we notice that the distinction becomes less obvious indicating the greater sensitivity of the Smag2D to the change of L_h.

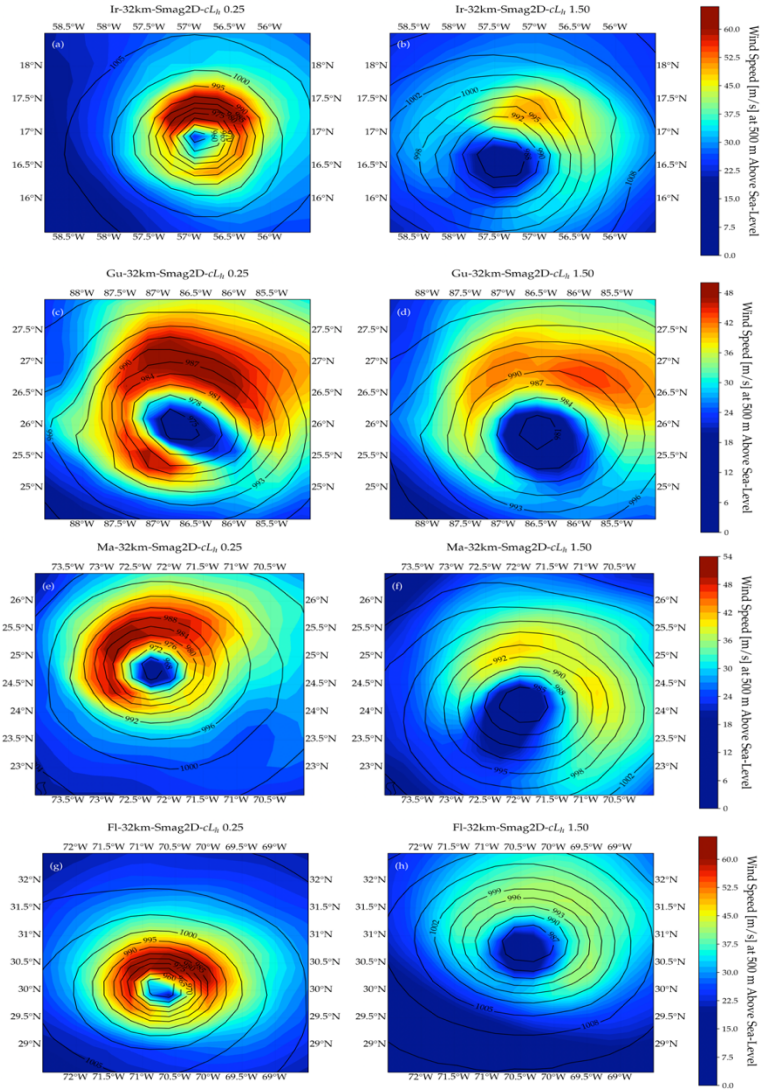

Figure S.5.1. Contour maps showing the wind speed at 500 meter above the sea level with isobars depicting the sea-level pressure for grid size of 32 km for hurricanes Irma (after 34 hours of simulation), Gustav (after 16 hours of simulation), Maria (after 12 hours of simulation) and Florence (after 34 hours of simulation). The left panels represent the Smag2D turbulence model with cL_h = 0.25 and the right panels display the same turbulent model with cL_h = 1.5.

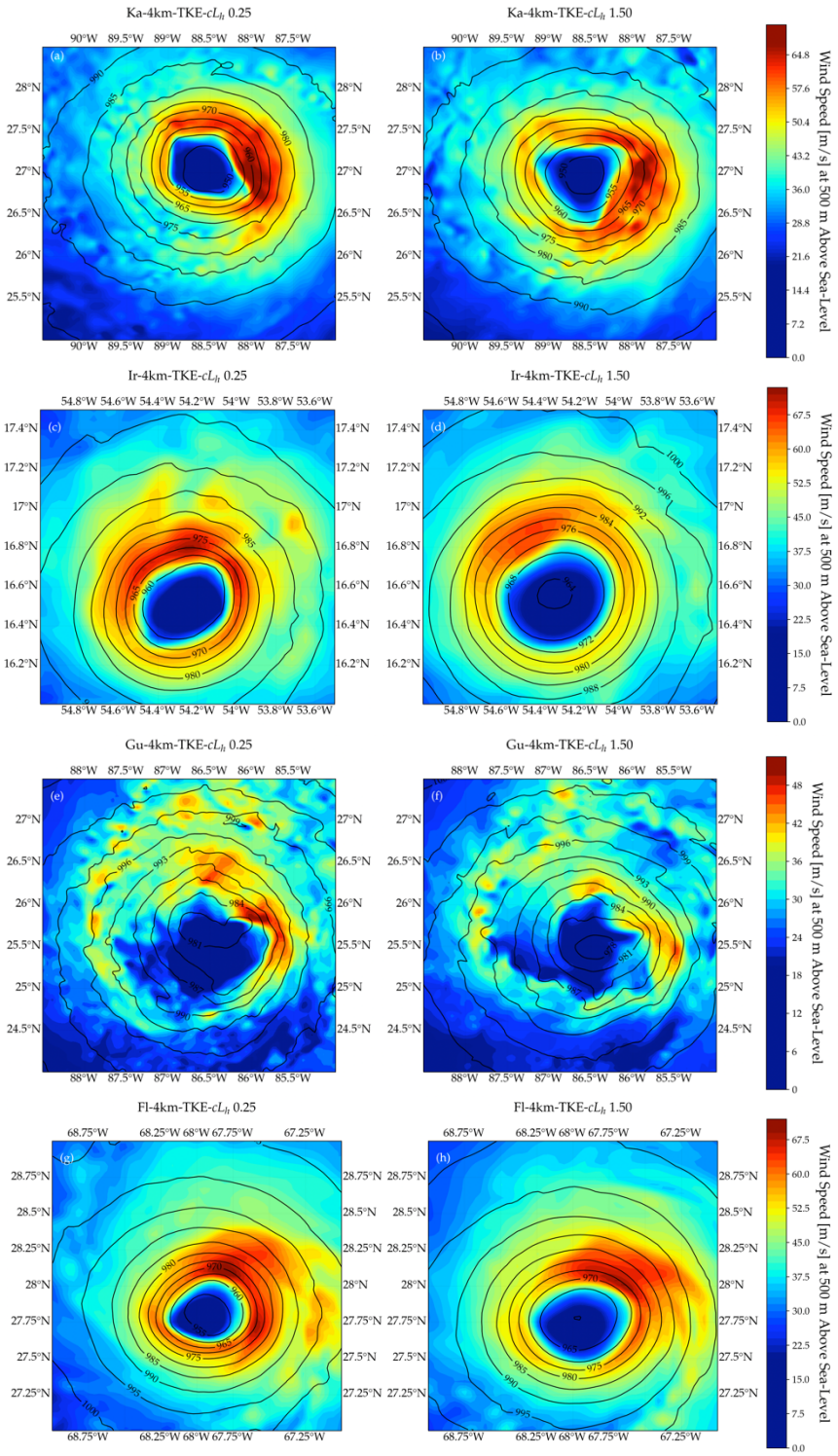

Figure S.5.2. Similar to Figure S.5.1 for WRF simulations with grid size of 4 km and TKE turbulence model.

Text S6. Wind speed versus distance to the hurricane center in terms of grid size, turbulence closure, and cL_h

To locate the eyewall radius for each simulation, figures S.5.1 – S.5.6 depict a one-hour temporal average of 10-meter wind speed in terms of radial distance and sea level pressure. These plots were then normalized in terms of the maximum wind speed, the maximum wind speed's radius and the maximum wind speed's sea-level pressure.

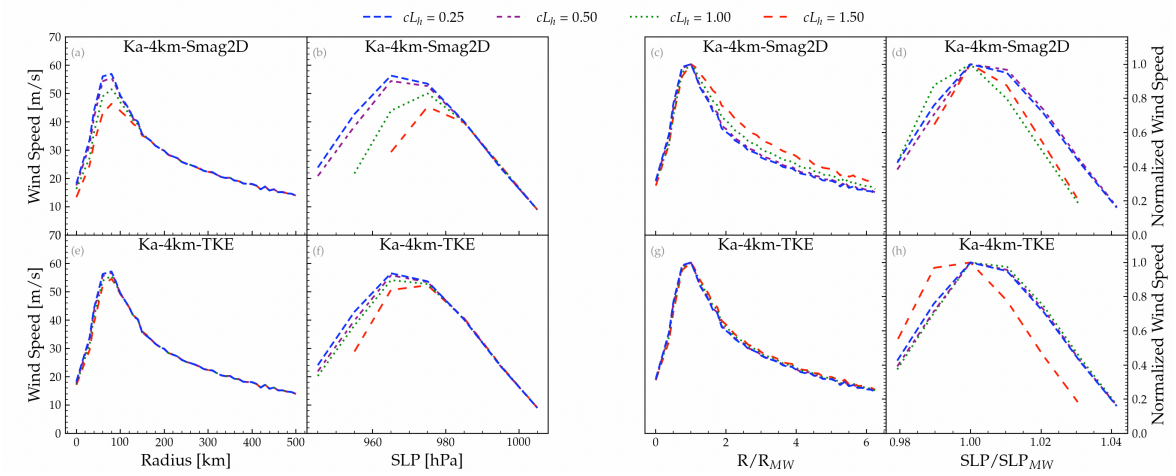

Figure S.6.1. A one-hour temporal average of 500 meters above sea-level wind speed in terms of both radial distance to the hurricane's eye and sea-level pressure for hurricane Katrina for the grid size of 4 km. (c,d,g,h) 500-meters wind speed is normalized by the maximum wind speed (V/Vmax), the radius is normalized by the maximum wind speed's radius (R/RMW) and the sea-level pressure is normalized by the maximum wind speed's sea-level pressure (SLP/SLPMW).

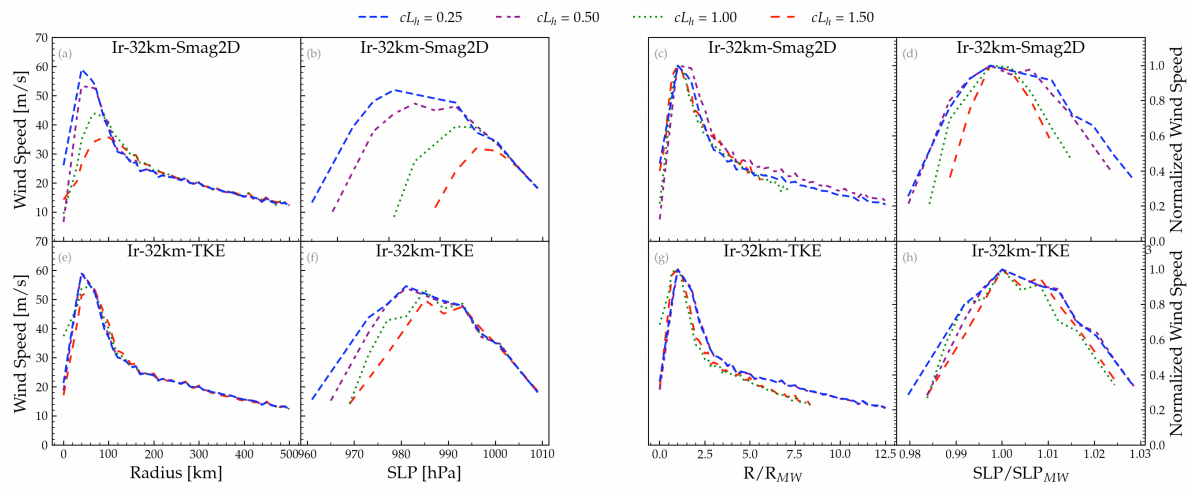

Figure S.6.2. Similar to Figure S.6.1 for Hurricane Irma and the grid size of 32 km.

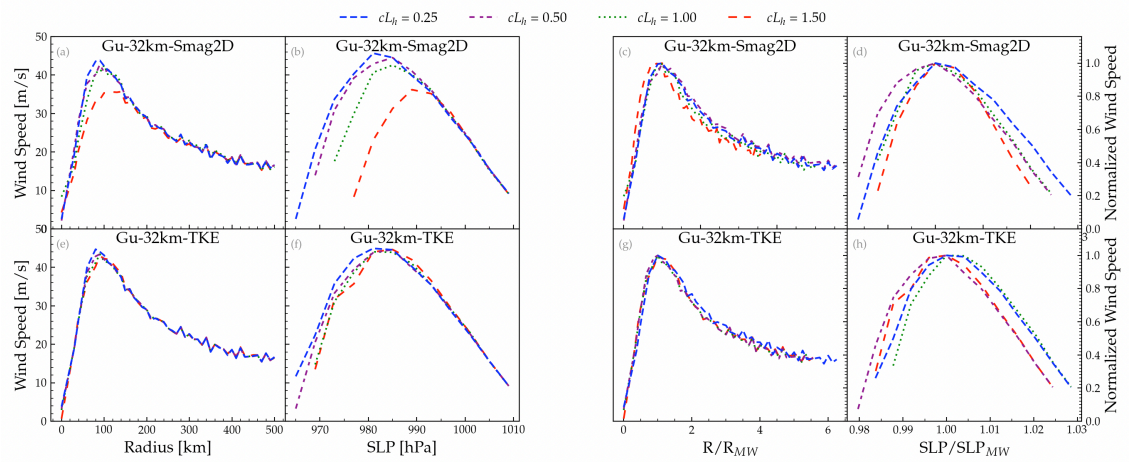

Figure S.6.3. Similar to Figure S.6.1 for Hurricane Gustav and the grid size of 32 km.

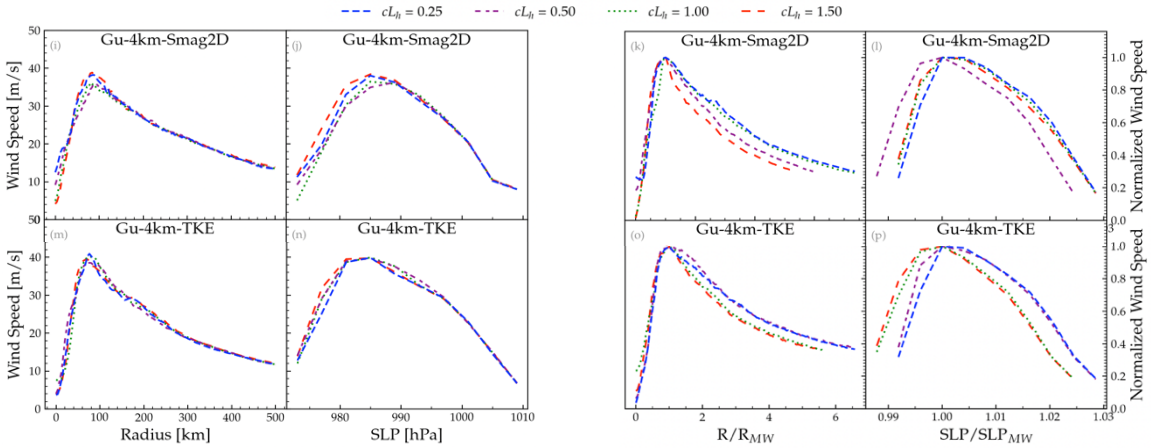

Figure S.6.4. Similar to Figure S.6.1 for Hurricane Gustav.

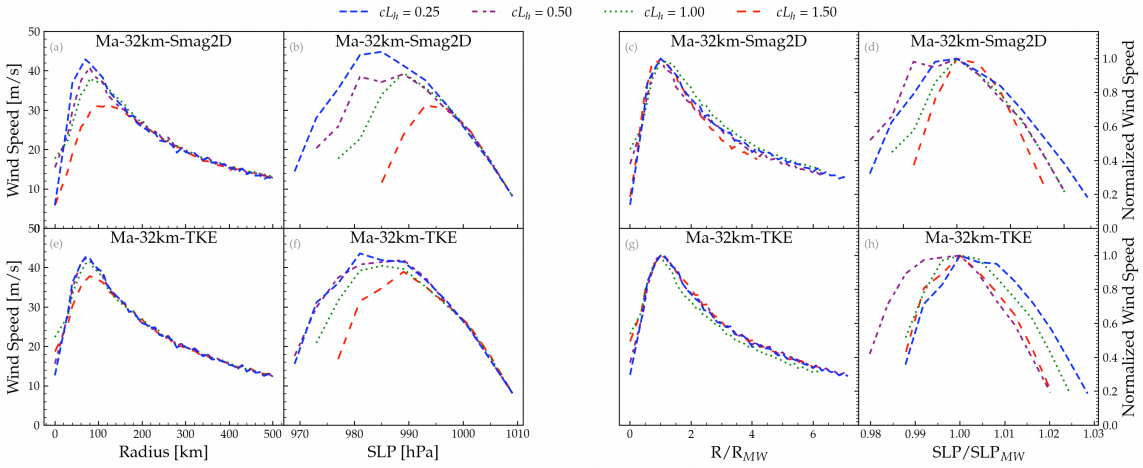

Figure S.6.5. Similar to Figure S.6.1 for Hurricane Maria and the grid size of 32 km.

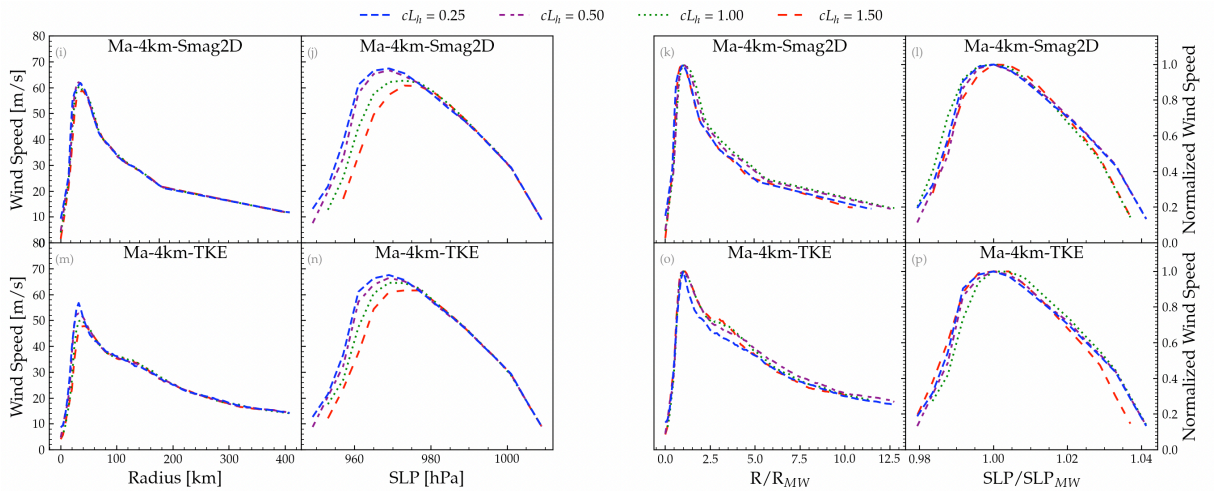

Figure S.6.6. Similar to Figure S.6.1 for Hurricane Maria.

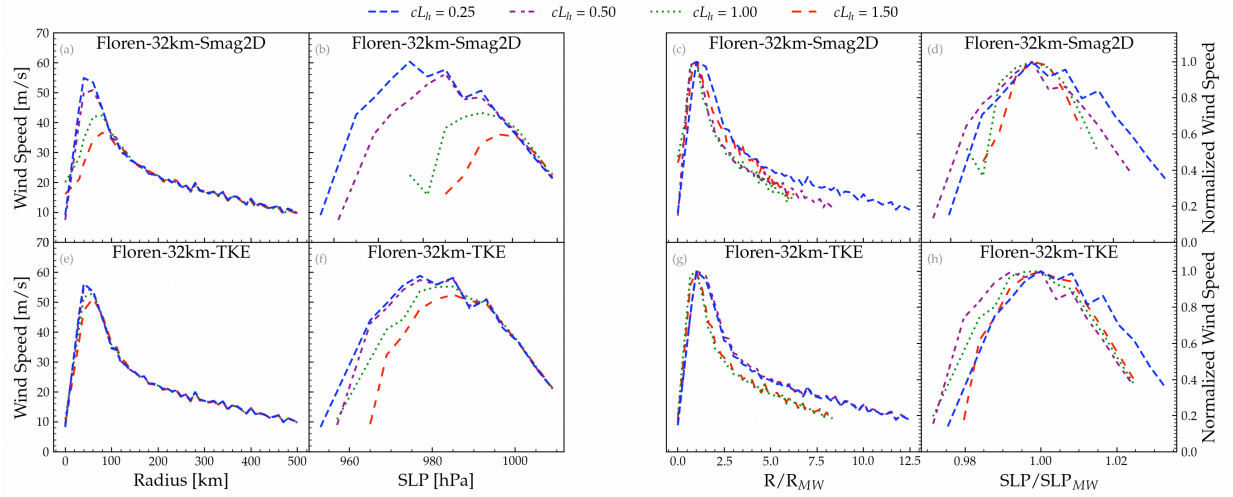

Figure S.6.7. Similar to Figure S.6.1 for Hurricane Florence and the grid size of 32 km.

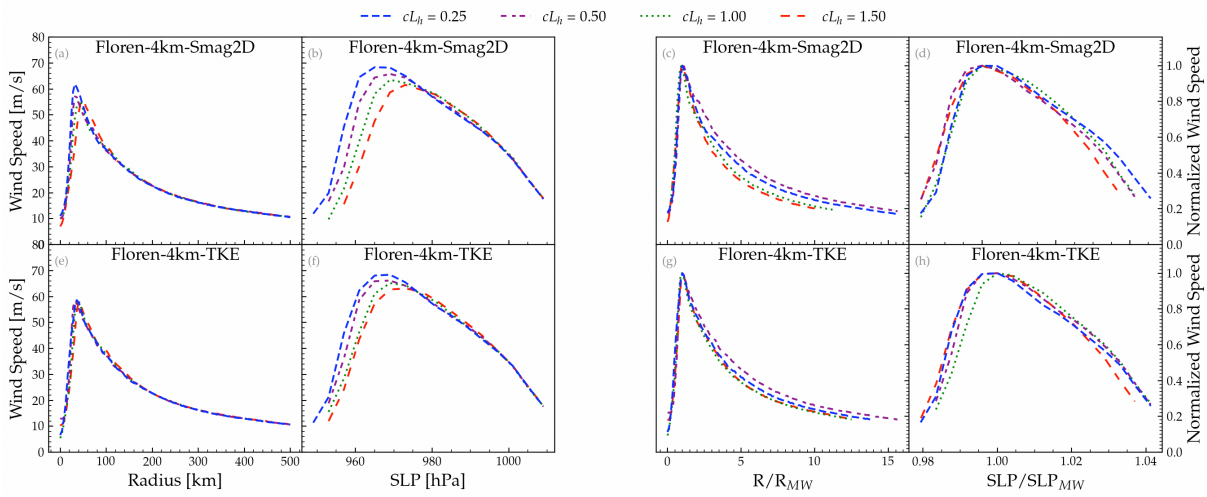

Figure S.6.8. Similar to Figure S.6.1 for Hurricane Florence.

A general trend is observed where decreasing the mixing length scale leads to an increase of the average and maximum wind speed and a decrease of the minimum sea level pressure. The Smag2D model is more sensitive to this change in comparison with the TKE.

Text S7. Impacts of horizontal mixing length on hurricane size and average maximum wind intensity

Changing the horizontal mixing length impacts hurricane intensity as well as its size. To assess the impact of horizontal mixing length on these factors, the maximum wind intensity and the average radius of maximum wind intensity based are calculated for 70% of the available time steps by removing the first few steps. In agreement with the results presented in S6, decreasing the horizontal mixing length generally tends to increase the average maximum wind intensity and decrease the average radius of maximum wind intensity (size of hurricane) regardless of the grid resolution or the turbulence model.

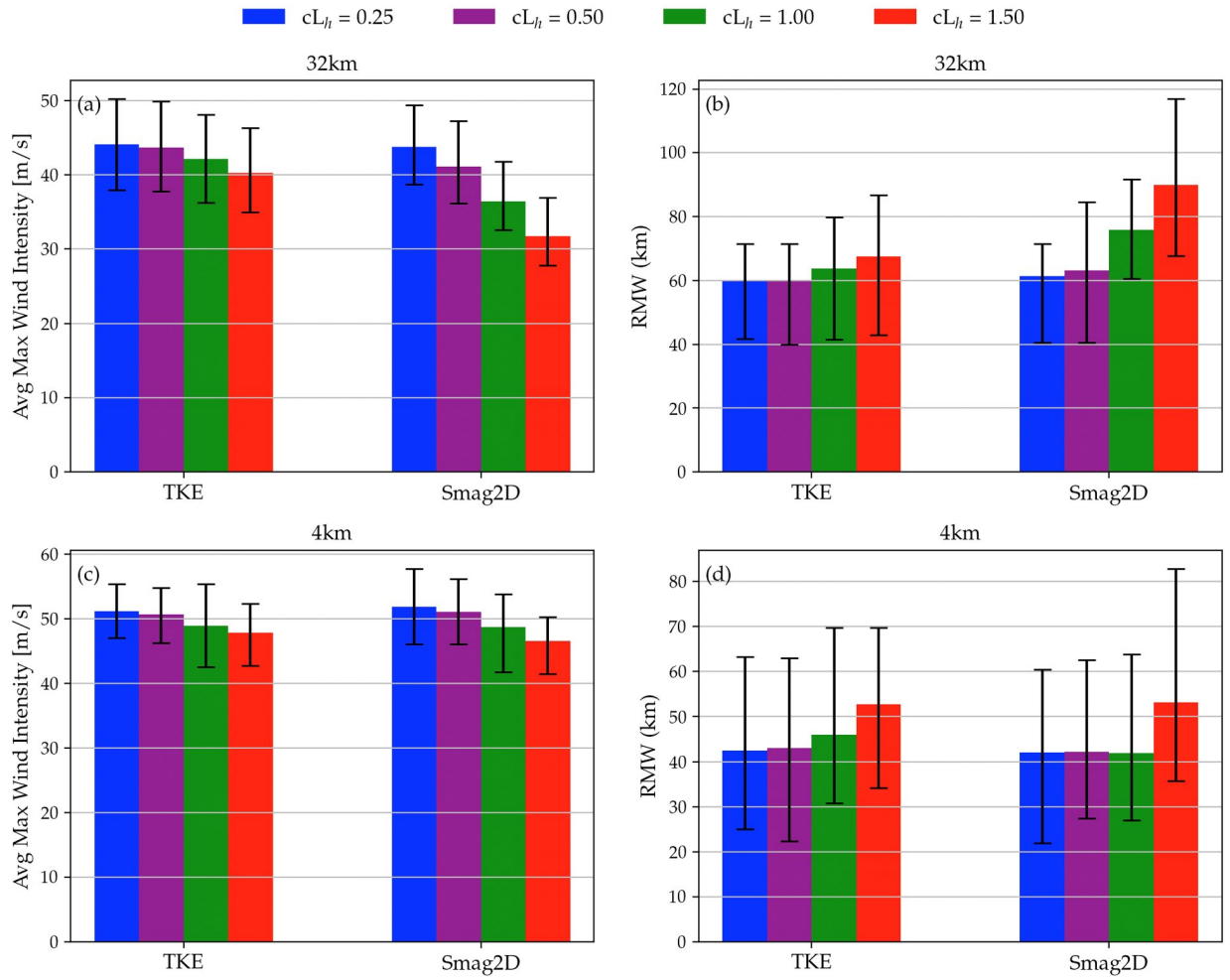

Figure S.7: Average maximum wind intensity and radius of maximum wind (RMW) in terms of length scales and turbulence models for 32 and 4 km grid sizes. The solid black lines represent the 10th and 90th percentiles intervals.

Text S8. Hurricane wind profiles in terms of grid size, turbulence closure, and cL_h

Figures S.8.1 – S.8.5 depict the wind profiles before and after the eyewall for all hurricanes with Smag2D and TKE turbulence models. Overall, the results show that reducing the cL_h increases the maximum wind speed.

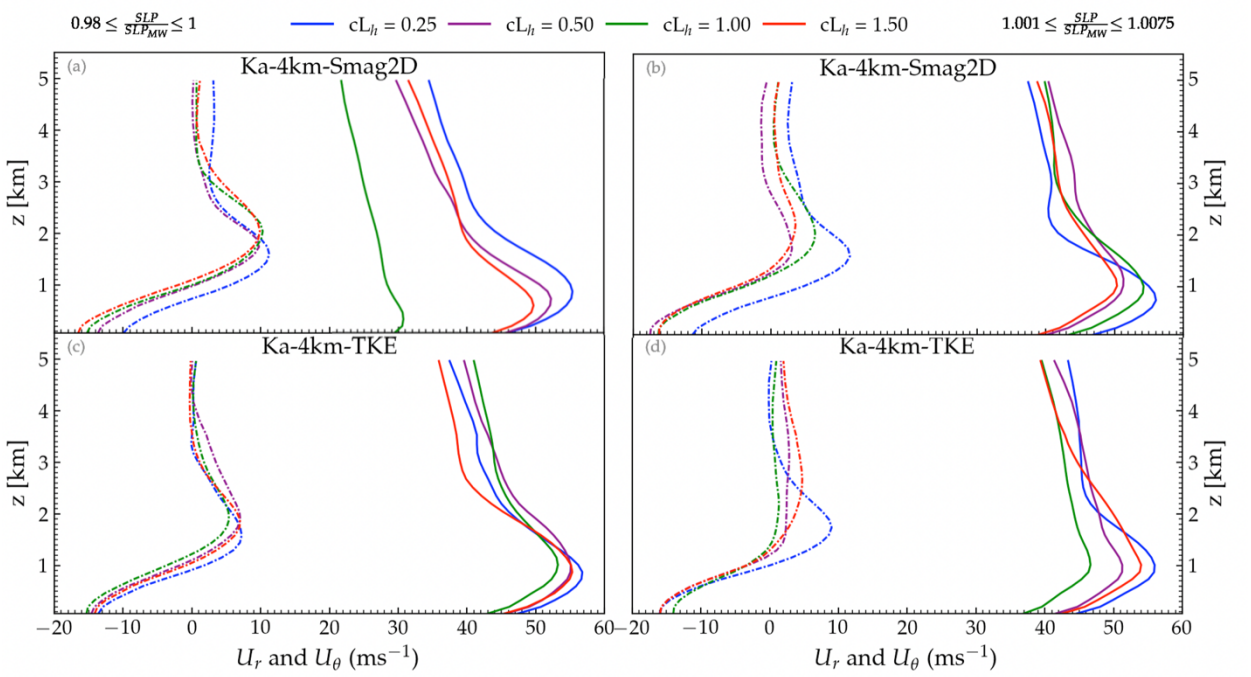

Figure S.8.1. A one-hour temporal average of the radial (U_r) and tangential (U_θ) wind profiles for different turbulence models and length scales. For hurricane Katrina, a grid size of 4km was employed.

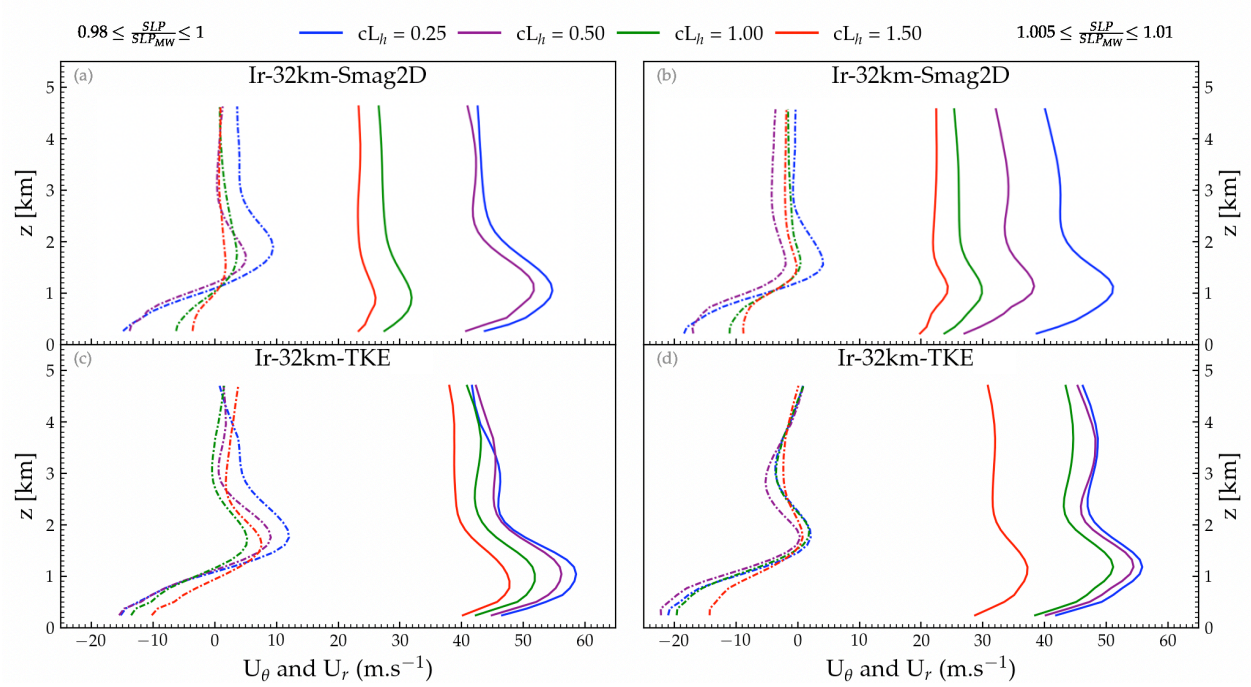

Figure S.8.2. A one-hour temporal average of the radial and tangential wind profiles for different turbulent models and length scales. For hurricane Irma, a grid size of 32km was employed.

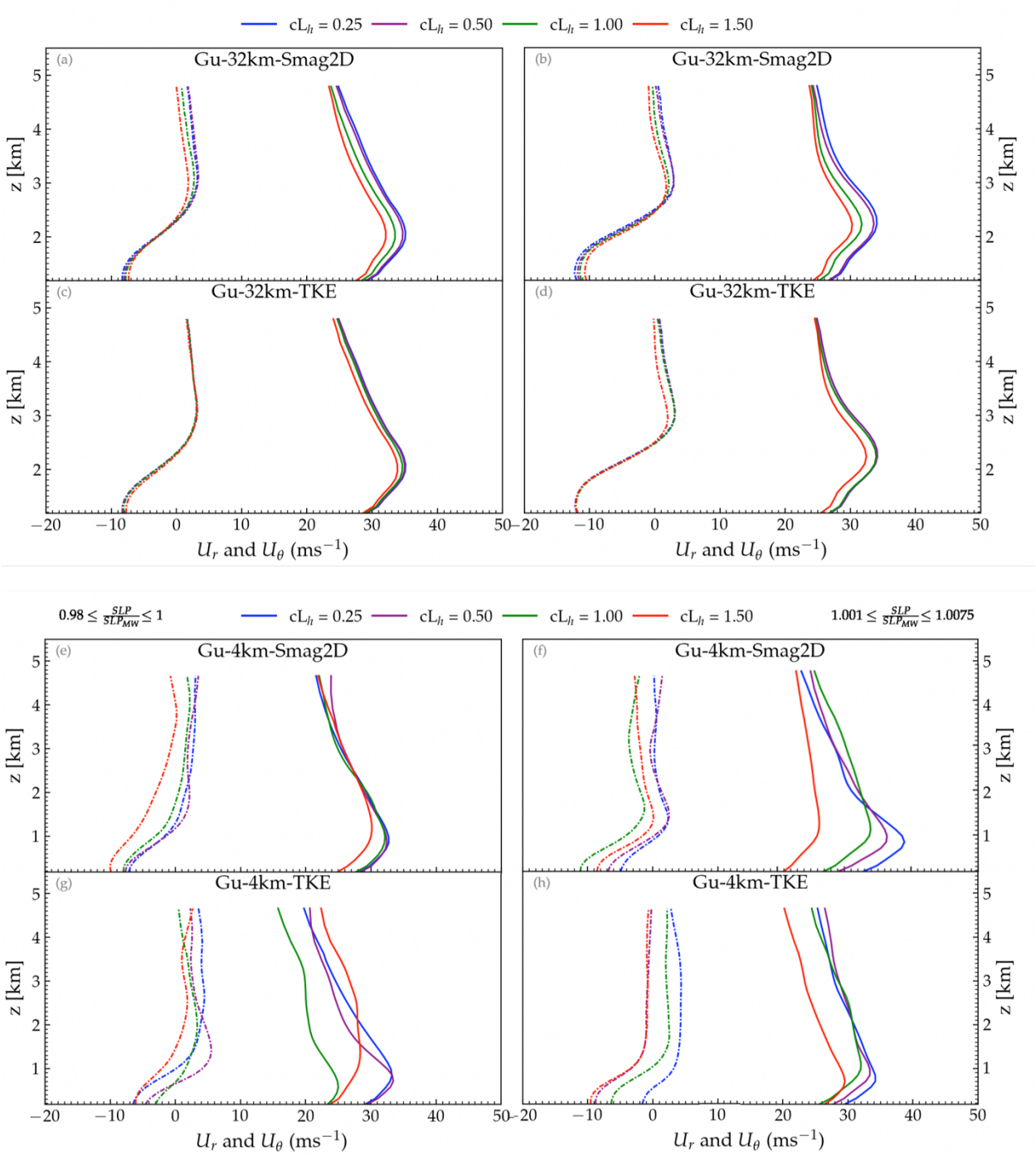

Figure S.8.3. A one-hour temporal average of the radial and tangential wind profiles for different turbulence models and length scales. For hurricane Gustav, a grid size of 32 km (top) and 4km (bottom) were employed.

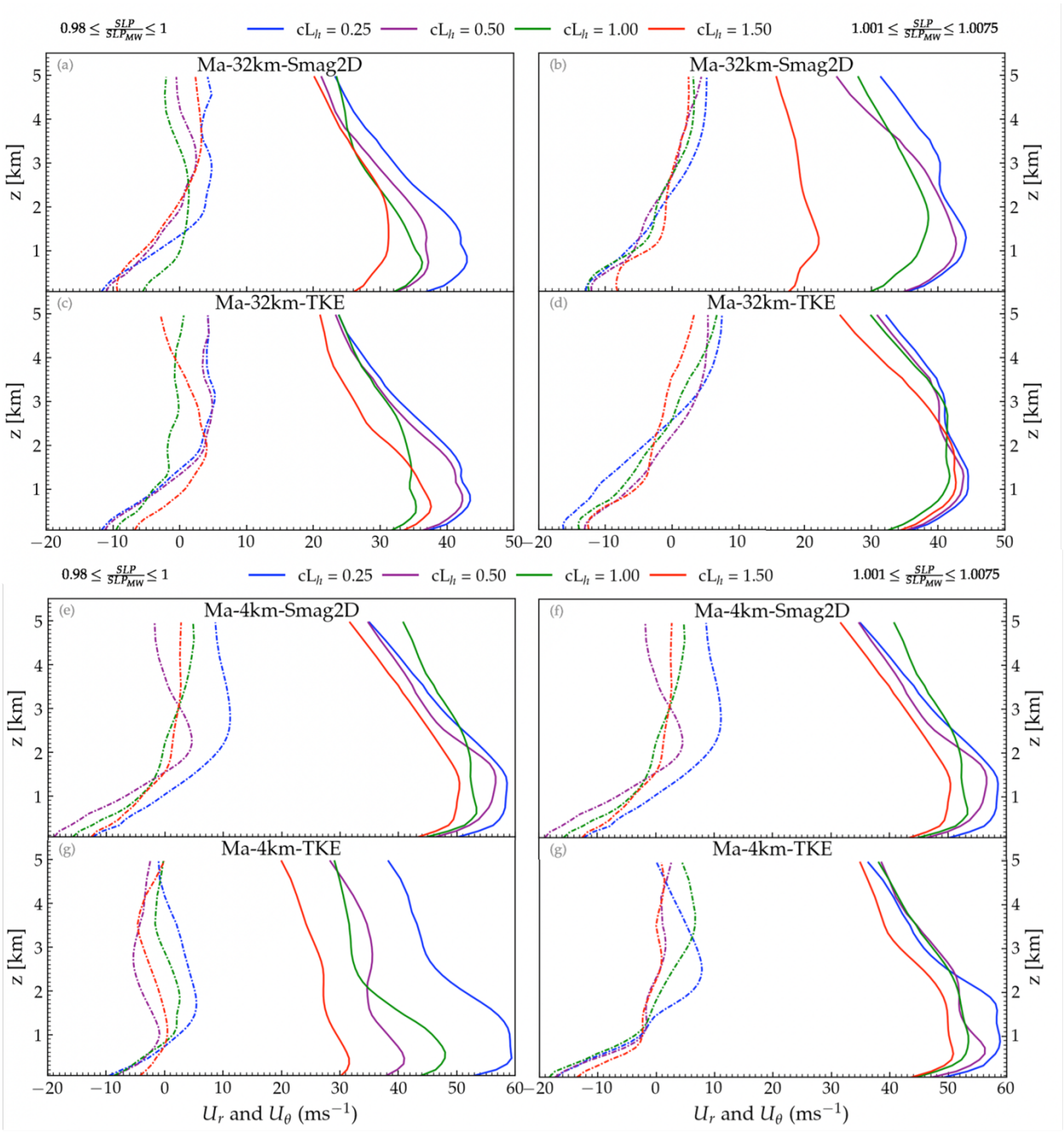

Figure S.8.4. A one-hour temporal average of the tangential (U_θ) and radial (U_r) wind profiles for different turbulence models and length scales. For hurricane Maria, a grid size of respectively 32 km (top) and 4km (bottom) were employed.

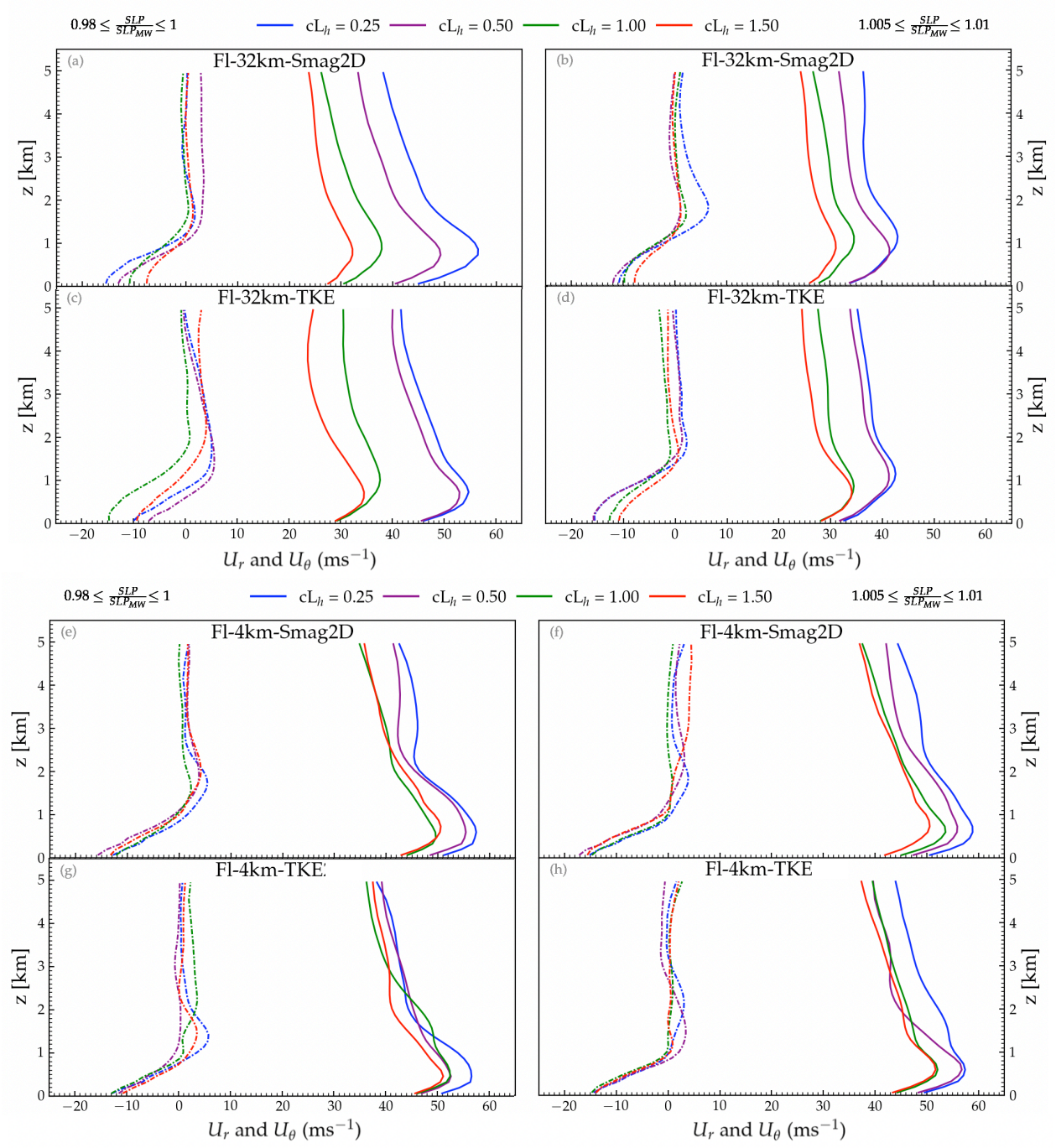

Figure S.8.5. A one-hour temporal average of the tangential (U_θ) and radial (U_r) wind profiles for different turbulence models and length scales. For hurricane Florence, a grid size of respectively 32 km (top) and 4km (bottom) were employed.

Text S9. The impacts of changing L_h on radial and tangential wind contours

Changing the horizontal mixing length impacts both the tangential and radial wind velocities. In figures S.9.1-S.9.3, we show the radial and tangential wind contours in the south-north cross section of each hurricane simulated using Smag2D and TKE turbulence schemes at 32 km and 4 km grid resolutions. In general, the radial wind intensity contours indicate larger inflow (darker blue in the first and third rows) and outflow (darker red in the 1st and 3rd rows) as we decrease the L_h. These will speed up the hurricane vortex and hence intensifies the tangential winds.

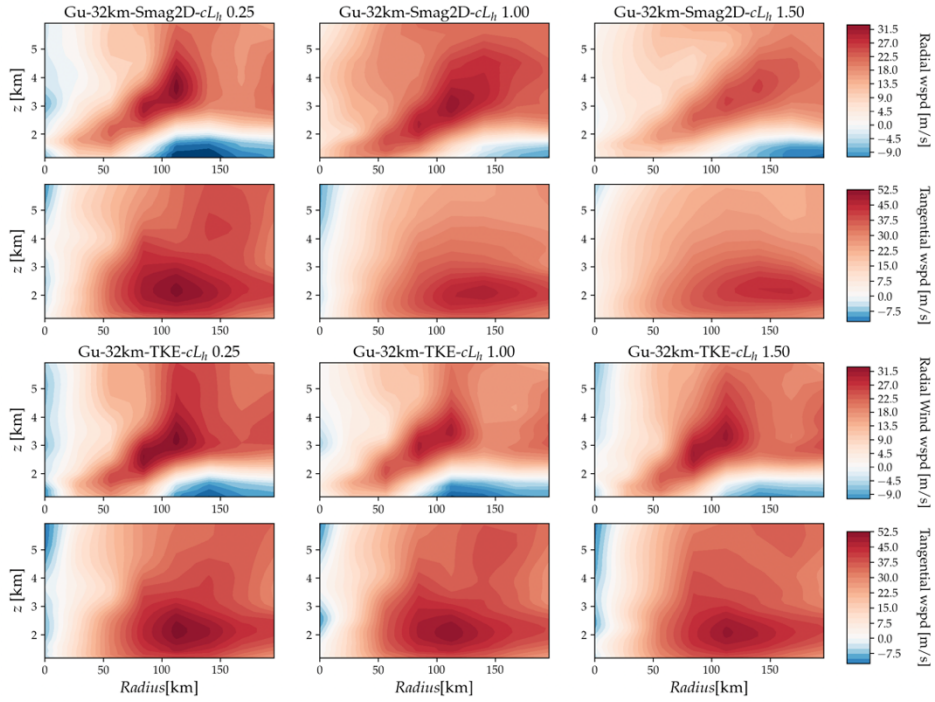

Figure S.9.1. Radial and tangential wind contours in the south-north cross section of hurricane Gustav (12 hours of simulation) for different turbulence models and a grid size of 32 km.

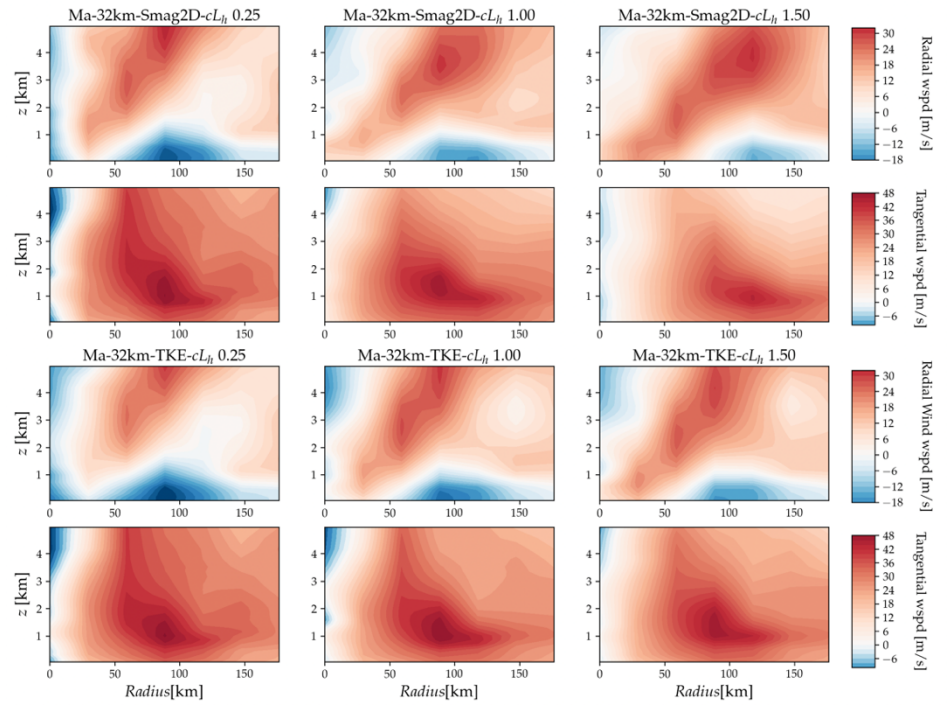

Figure S.9.2. Radial and tangential wind contours in the south-north cross section of hurricane Maria (12 hours of simulation) for different turbulence models and a grid size of 32 km.

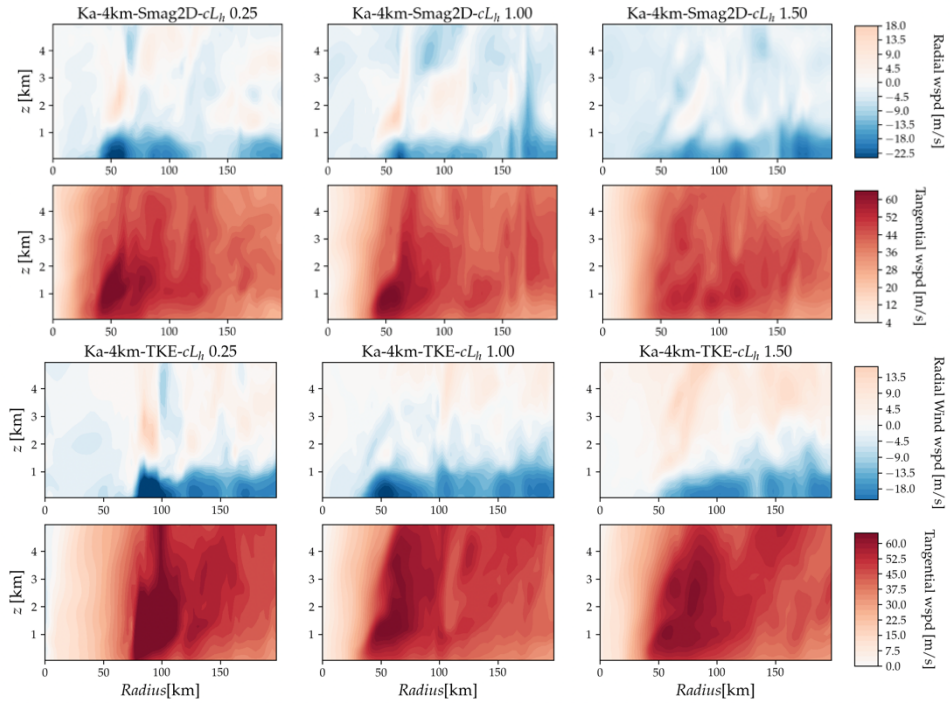

Figure S.9.3. Radial and tangential wind contours in the south-north cross section of hurricane Katrina (29 hours of simulation) for different turbulence models and a grid size of 4 km.

Text S10. Momentum budget balance

To better understand the impact of horizontal mixing length on the dynamics of the simulated hurricanes, the momentum budget terms are calculated. Figures S.10.1-S.10.2 display the vertical profile of the radial momentum budget of the hurricanes simulated using Smag2D and TKE models. The radial momentum budget is obtained using approximations for the radial momentum equation as follows similar to (Bryan et al., 2017):

$$\frac{\partial u_r}{\partial t} + u_r\frac{\partial u_r}{\partial r} + \frac{u_\theta}{r}\frac{\partial u_r}{\partial \theta} - \frac{u_\theta^2}{r} + u_z\frac{\partial u_r}{\partial z} = -\frac{1}{\rho}\frac{\partial p}{\partial r} + fu_\theta - \frac{\partial \overline{u_r' u_z'}}{\partial z} + \frac{\overline{u_\theta' u_\theta'}}{r} - \frac{1}{r}\frac{\partial r\overline{u_r' u_r'}}{\partial r} \quad (14)$$

where the radial advection is given by the 2nd term in the LHS ($u_r\frac{\partial u_r}{\partial r}$) of equation 14 ($\approx \frac{u_r^2}{R}$ in the radial direction), the centrifugal acceleration is defined by the 4th term ($\frac{u_\theta^2}{r}$ in the radial direction), the Coriolis acceleration is given by fu_θ, the pressure gradient acceleration $-\frac{1}{\rho}\frac{\partial P}{\partial r}$, and the rest of the terms are called the "residual (~diffusion)" which is $Residual = -\left[\frac{\partial u_r}{\partial t} + \frac{u_\theta}{r}\frac{\partial u_r}{\partial \theta} + u_z\frac{\partial u_r}{\partial z} + \frac{\partial \overline{u_r' u_z'}}{\partial z} - \frac{\overline{u_\theta' u_\theta'}}{r} + \frac{1}{r}\frac{\partial r\overline{u_r' u_r'}}{\partial r}\right]$ and is mainly dominated by the diffusion.

The decrease of the horizontal mixing length reduces $\tau_{\theta\theta}$, τ_{rr}, and $\tau_{\theta r}$ in the residual (~diffusion) term. This will modulate the force balance. For the same pressure gradient force, reducing the horizontal mixing length implies a smaller diffusion (lower Reynolds stresses as shown in figures 9 and S.11.1-S.11.5). Hence, as shown in figures S.10.1 and S.10.2 the diffusion term is decreased when the horizontal mixing length decreases in the presence of a relatively similar pressure gradient force. To compensate for this decrease in the diffusion, the centrifugal and Coriolis forces need to increase for a given similar pressure gradient. The result of this decrease in horizontal mixing length, as discussed throughout the paper, is the increase of the wind intensity in hurricanes.

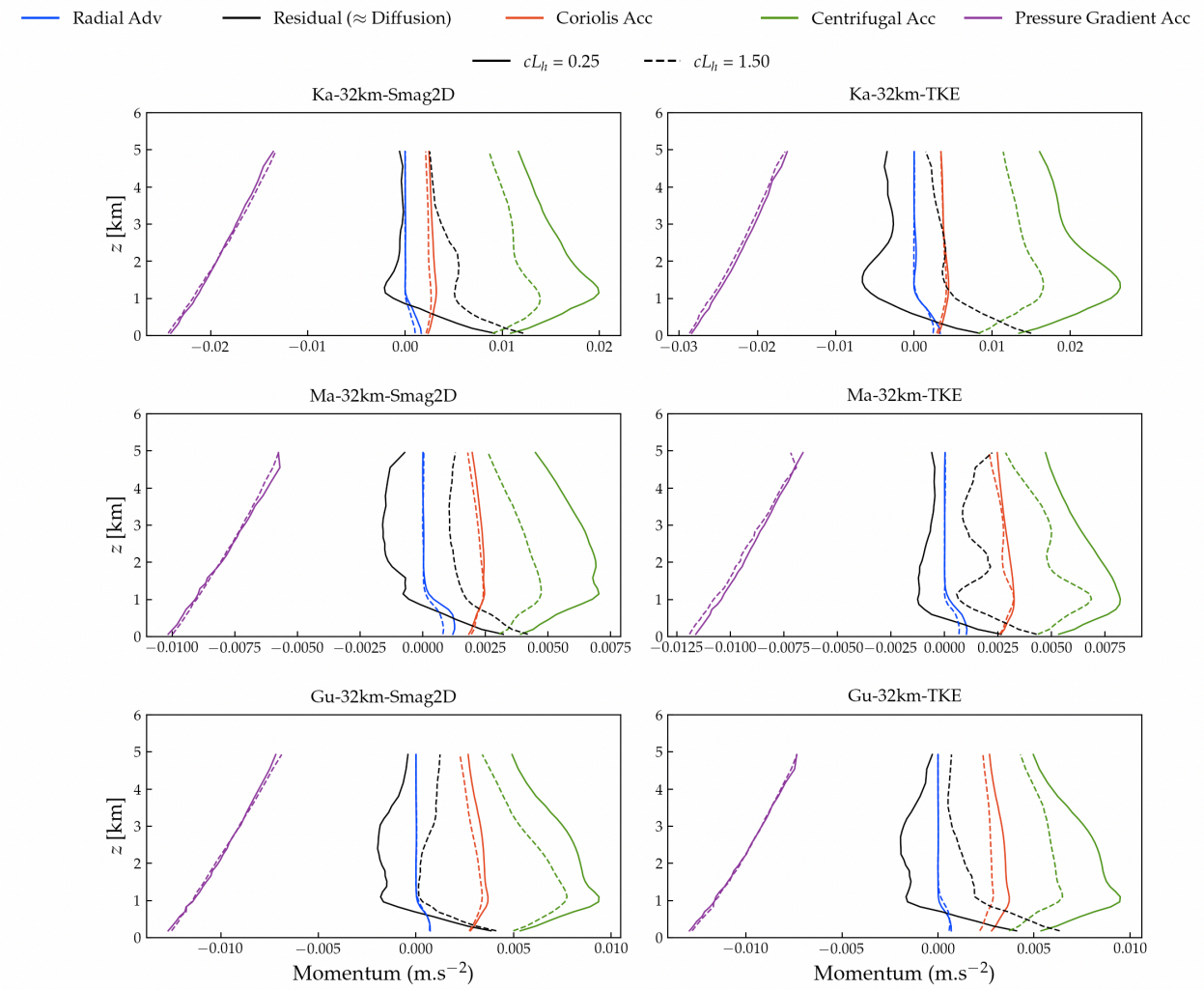

Figure S.10.1 The vertical profile of the radial momentum budget outside the eyewall region of all hurricanes simulated with Smag2D and TKE turbulence models over 32 km grid sizes. The data are extracted after 6-30 hours of simulations for Hurricanes Katrina, Gustav, and Maria.

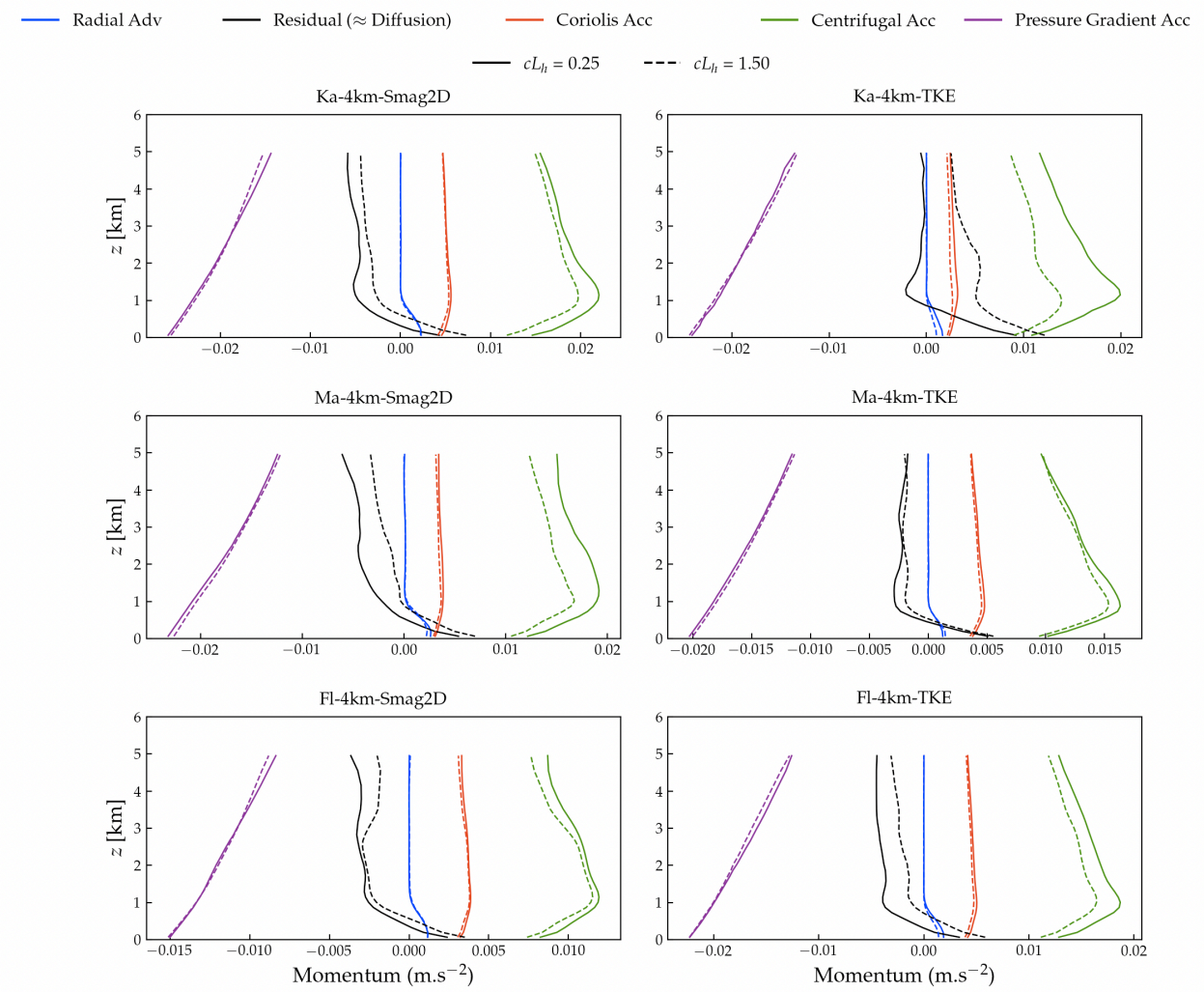

Figure S.10.2 Vertical profile of radial momentum budget outside the eyewall region of all hurricanes simulated with Smag2D and TKE turbulence models over 4 km grid sizes. The data are extracted after 12-24 hours of simulations for Hurricanes Katrina, Maria, and Florence.

Text S11. Reynolds stresses in terms of turbulence closure, grid size and cL_h

To investigate the mixing length scale impacts on the hurricane dynamics, the Reynolds stresses in the inner and outer eyewall region for all hurricanes are displayed in figures S.11.1 – S.11.5. An increase of cL_h yields to larger Reynolds stresses and produces more dissipation.

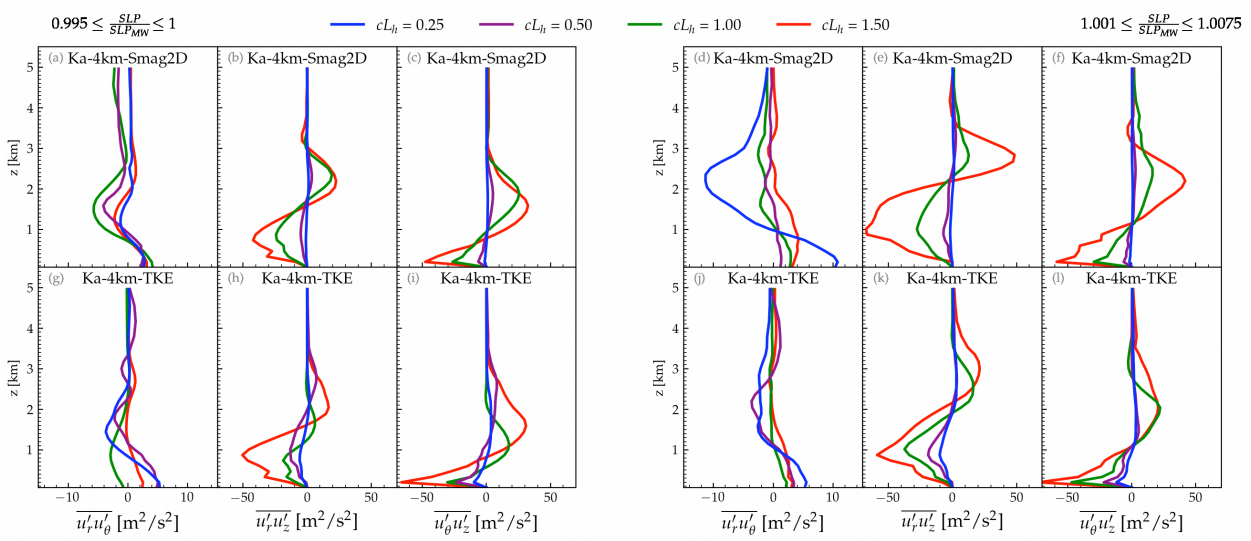

Figure S.11.1. One-hour temporal average of Reynolds' stresses for Hurricane Katrina, simulated with Smag2D and TKE turbulence models and 4km grid size.

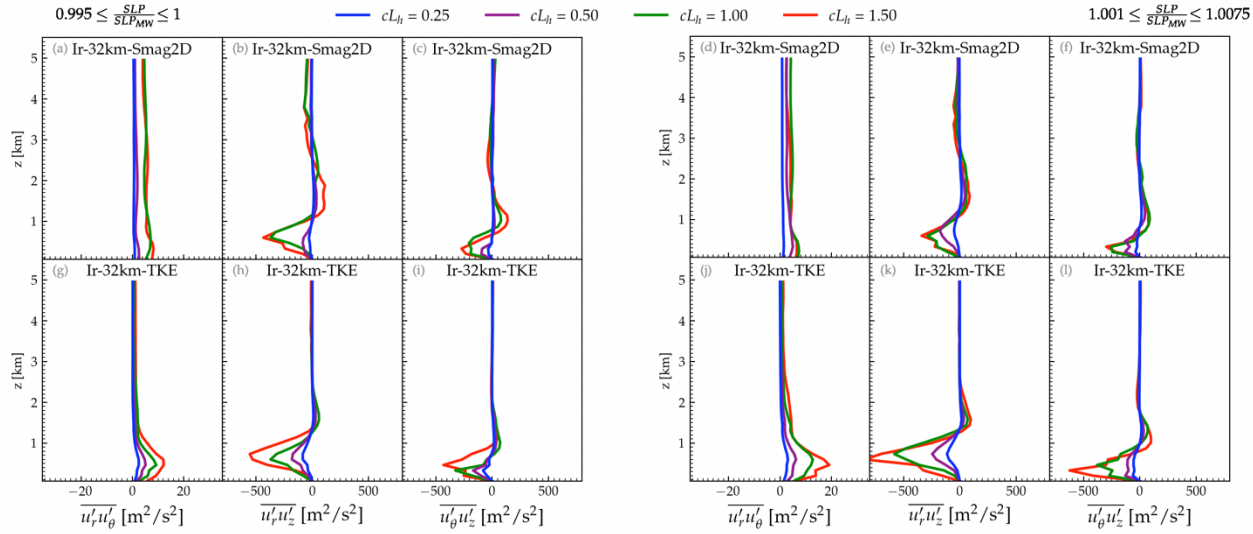

Figure S.11.2. One-hour temporal average of Reynolds' stresses for Hurricane Irma, simulated with Smag2D and TKE turbulence models and 32km grid size.

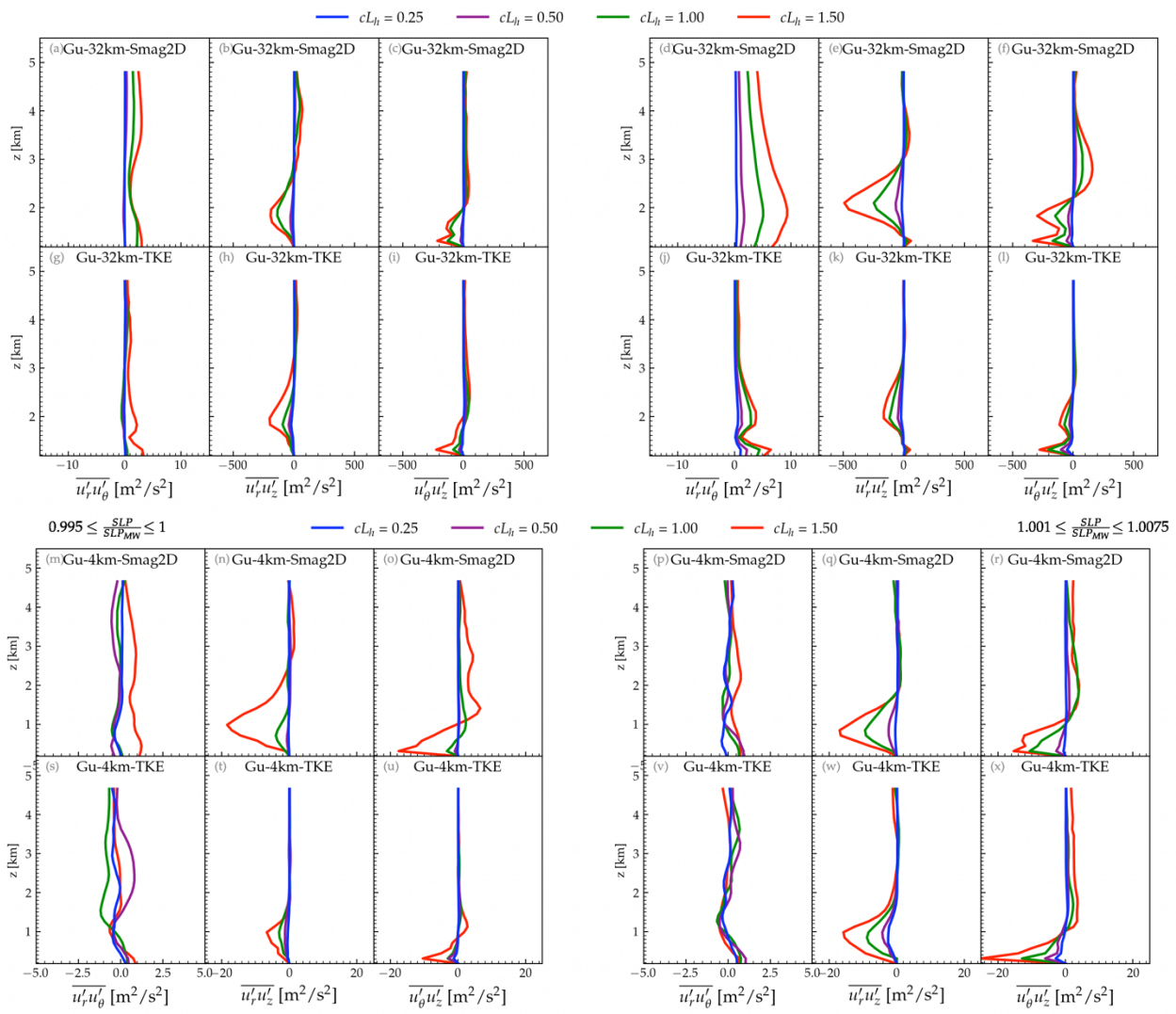

Figure S.11.3. One-hour temporal average of Reynolds' stresses for Hurricane Gustav, simulated with Smag2D and TKE turbulence models and 32km and 4km grid sizes.

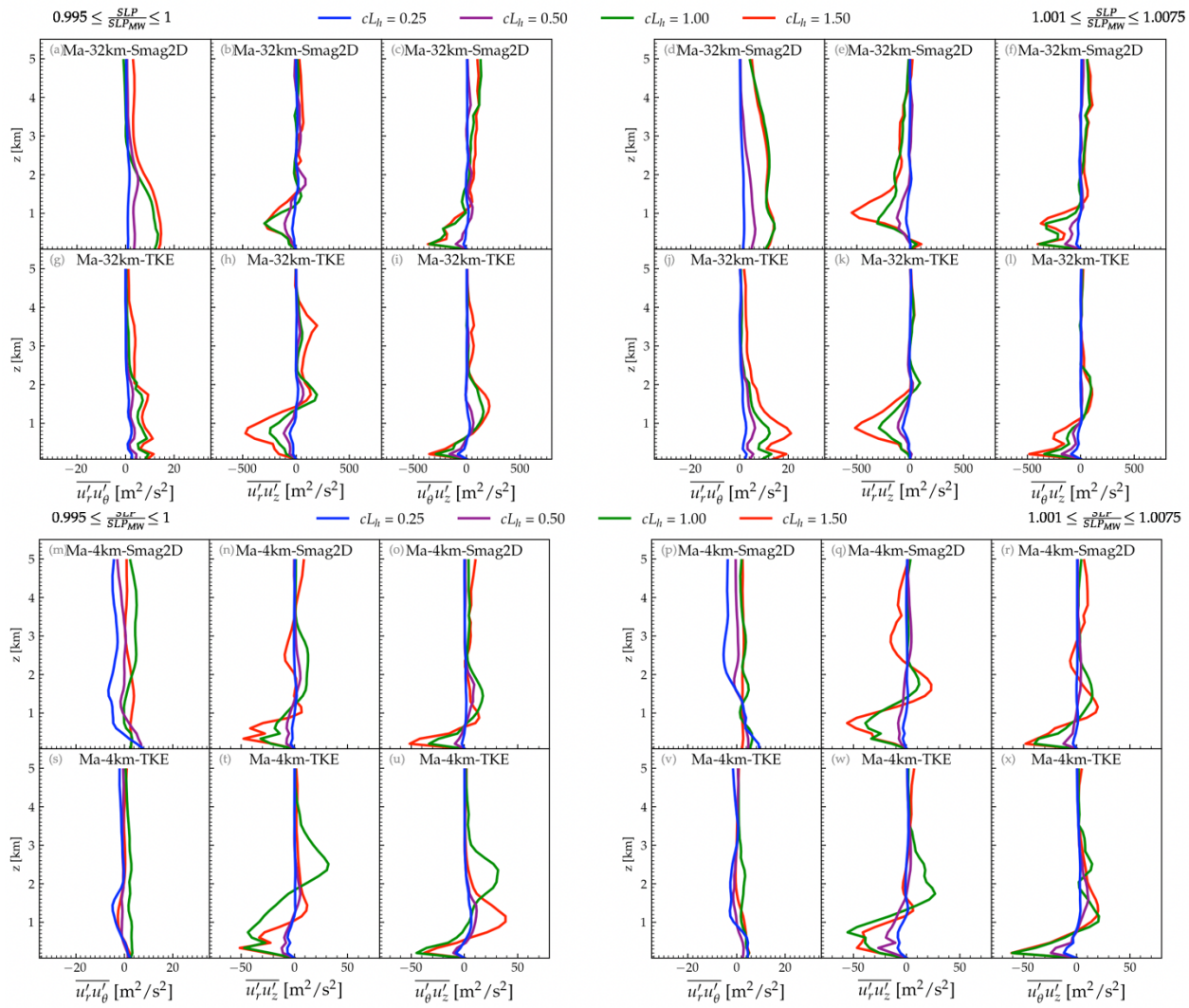

Figure S.11.4. One-hour temporal average of Reynolds' stresses for Hurricane Gustav, simulated with Smag2D and TKE turbulence models and 32km and 4km grid sizes.

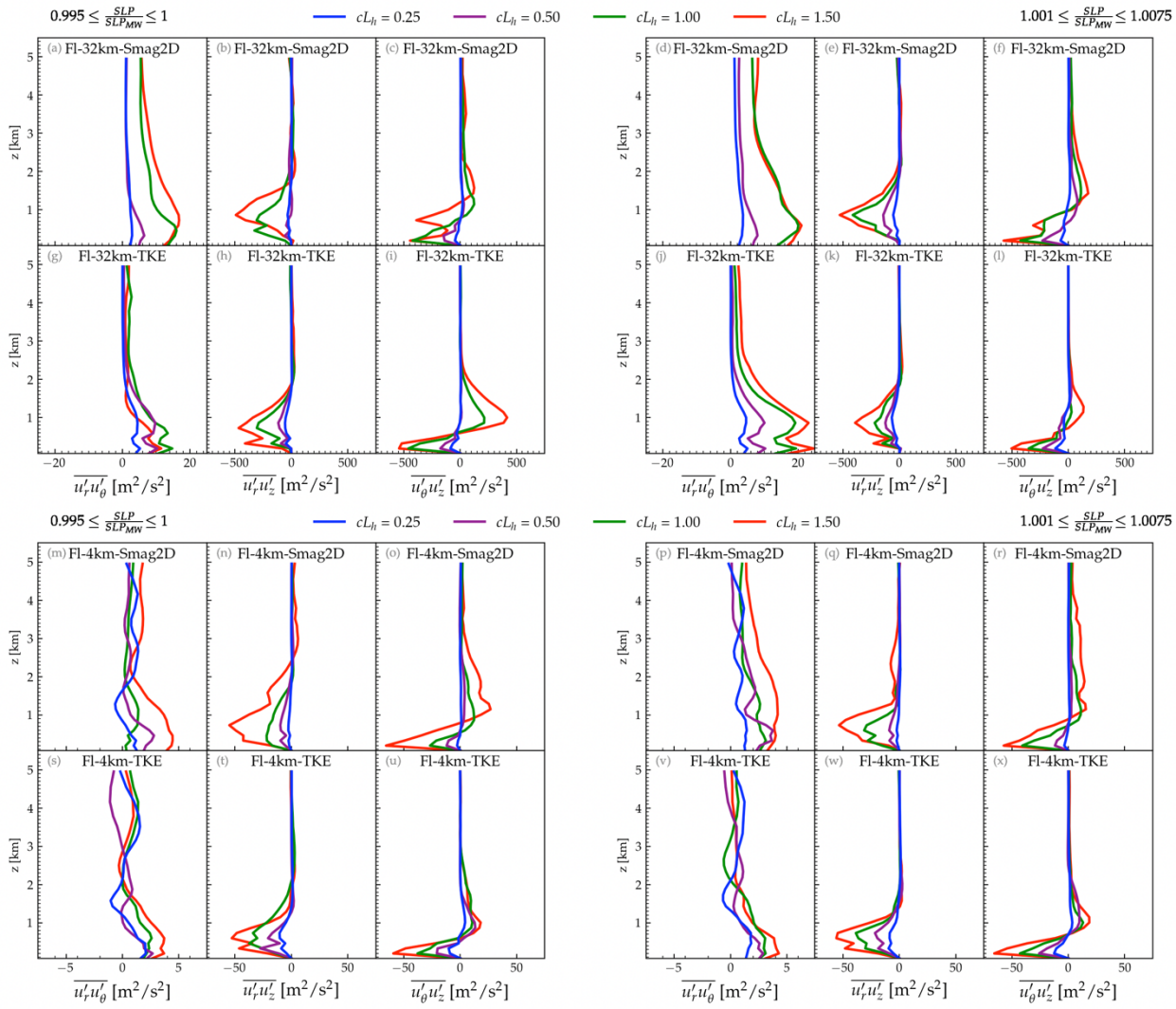

Figure S.11.5. One-hour temporal average of Reynolds' stresses for Hurricane Florence, simulated with Smag2D and TKE turbulence models and 32km and 4km grid sizes.

Text S12. The impacts of varying the horizontal mixing length on the accuracy of weak hurricanes simulations

To assess the impact of adjusting the horizontal mixing length on the forecasting accuracy of weak hurricanes, five hurricanes of categories 1 and 2 – Sally (2020), Jerry (2019), Helene (2018), Gordon (2012), and Nadine (2012) – were simulated using the Smag2D and TKE models for 32 and 4 km grid resolutions. The details of the simulated weak hurricanes are provided in table S4. The mixing length was changed for each simulation similar to the main paper. In total, 40 simulations were conducted.

Table S4. List of the investigated hurricanes and their simulation periods in WRF.

Hurricanes	Year	Category	Formation to Dissipation Dates	Simulation Running Hours	Approximate Domain Size	Observed Max Speed
Sally	2020	2	Sept. 11 – Sept. 17	36 h, Sept. 14, 12 pm – Sept. 16, 12 am	2240 km × 2240 km	49 m/s
Jerry	2019	2	Sept. 17 – Sept. 24	36 h, Sept. 19, 12 pm – Sept. 21, 12 am	2240 km × 2240 km	46 m/s
Helene	2018	2	Sept. 7 – Sept. 16	72 h, Sept. 10, 12 am – Sept. 13, 12 am	2240 km × 2240 km	49 m/s
Gordon	2012	2	Aug. 15 – Aug. 20	48 h, Aug. 18, 6 am – Aug. 20, 6 am	2240 km × 2240 km	49 m/s
Nadine	2012	1	Sept. 10 – Oct. 3	48 h, Sept. 14, 6 pm – Sept. 16, 6 pm	2240 km × 2240 km	41 m/s

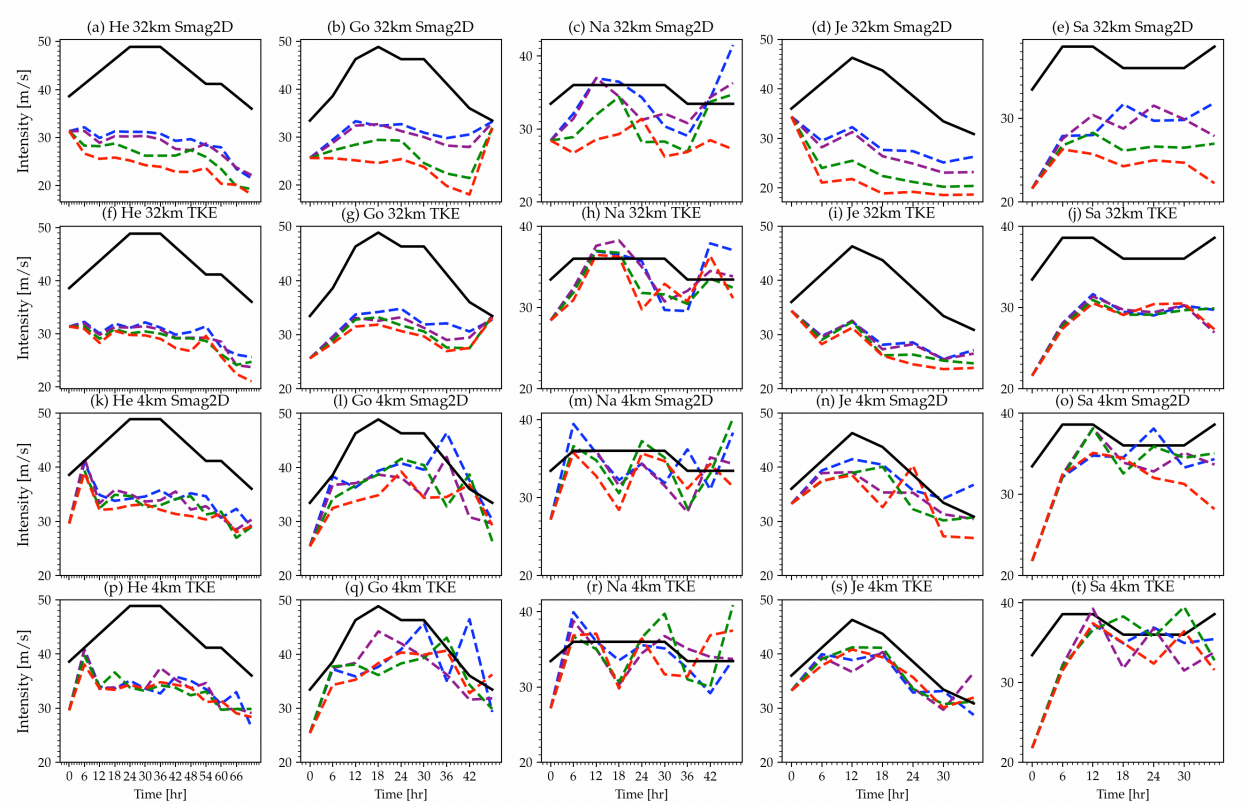

Figure S.12.1: Smag2D and TKE forecasted near-surface wind speed (10 m of altitude) timeseries among all considered category 1 and 2 hurricanes, for 32 km and 4 km grid sizes and for different L_h values. The solid black line represents the best track wind speed based on observations.

The time series of the near-surface wind intensity for all simulations are provided in figure S.2.1. For 32 km grid resolution, both models generally underestimate the wind intensity and the decrease of L_h yields higher intensities. For the finer grid size, the decrease of L_h had a similar impact on the wind intensity. To better characterize the impacts of adjusting the L_h values on the forecasting accuracy of weak hurricanes, we depict the $MAPE_{Intensity}$ and MAE_{Track} of all conducted simulations in figure S.12.2.

The results suggest a similar finding to that observed for strong hurricanes: lower horizontal mixing length generally improves the wind intensity forecasts in the considered weak hurricane. Similarly, Smag2D is more sensitive to L_h changes in the considered weak hurricanes than the TKE model. On average, the decrease of the default horizontal mixing length by a

coefficient of 0.25 improved the intensity predictions by 7.2% (5.4%) and 26.2% (6.9%) for TKE and Smag2D over the 32 km (4 km) grid resolution, respectively.

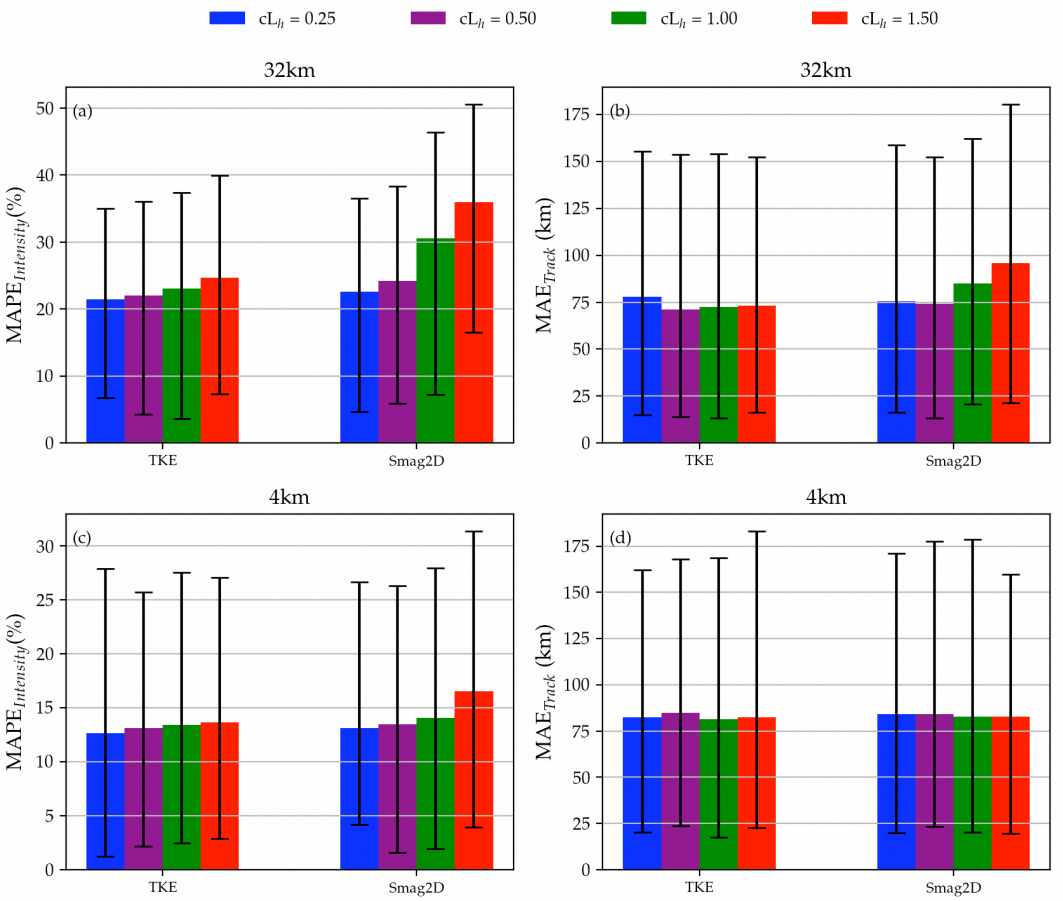

Figure S.12.2: Average error of all hurricanes in terms of length scales and turbulence models for 32 and 4 km grid sizes. The solid black lines represent the 10th and 90th percentiles intervals.

References

Beven II, J. L., & Kimberlain, T. B. (2009). Tropical Cyclone Report: Hurricane Gustav (2008). *Tropical Cyclone Report Hurricane Gustav*, 1–38.

Black, P. G., D'Asaro, E. A., Drennan, W. M., French, J. R., Niiler, P. P., Sanford, T. B., et al. (2007). Air-sea exchange in hurricanes. *Bull. Amer. Meteor. Soc.*, *88*, 357–374.

Bryan, G. H., Worsnop, R. P., Lundquist, J. K., & Zhang, J. A. (2017). A Simple Method for Simulating Wind Profiles in the Boundary Layer of Tropical Cyclones. *Boundary-Layer Meteorology*, *162*(3), 475–502. https://doi.org/10.1007/s10546-016-0207-0

Cangialosi, J. P., Latto, A. S., & Berg, R. (2018). Hurricane Irma. *National Hurricane Center Tropical Cyclone Report: Hurricane Irma*, 1–111.

Cavallo, S., Torn, R., Snyder, C., Davis, C., Wang, W., & Done, J. (2013). Evaluation of the Advanced Hurricane WRF data assimilation system for the 2009 Atlantic hurricane season. *Monthly Weather Review*, *141*(2), 523–541.

Davis, C., Wang, W., Chen, S. S., Chen, Y., Corboseiro, K., Demaria, M., et al. (2008). Prediction of Landfalling Hurricanes with the Advanced Hurricane WRF Model. *Monthly Weather Review*, 1990–2005. https://doi.org/10.1175/2007MWR2085.1

Donelan, M. A., Haus, B. K., Reul, N., Plant, W. J., Stiassnie, M., Graber, H. C., et al. (2004). On the limiting aerodynamic roughness of the ocean in very strong winds. *Geophysical Research Letters*, *31*(18), 1–5. https://doi.org/10.1029/2004GL019460

Dudhia, J. (1989). Numerical study of convection observed during the winter monsoon experiment using a mesoscale two-dimensional model. *Journal of the Atmospheric Sciences*, *46*(20), 3077-31–7.

Garratt, J. R. (1994). Review: the atmospheric boundary layer. *Earth Science Reviews*, *37*(1–2), 89–134. https://doi.org/10.1016/0012-8252(94)90026-4

Hong, S.-Y., Lim, K.-S., Kim, J.-H., Ock, J.-, Lim, J., & Dudhia, J. (n.d.). *WRF Single-Moment 6-Class Microphysics Scheme (WSM6)*.

Hong, S. (2010). A new stable boundary-layer mixing scheme and its impact on the simulated East Asian summer monsoon. *Quarterly Journal of the Royal Meteorological Society*, *136*(651), 1481–1496.

Hong, S. Y., Dudhia, J., & Chen, S. H. (2004). A revised approach to ice microphysical processes for the bulk parameterization of clouds and precipitation. *Monthly Weather Review*, *132*(1), 103–120. https://doi.org/10.1175/1520-0493(2004)132<0103:ARATIM>2.0.CO;2

Hong, S. Y., Noh, Y., & Dudhia, J. (2006). A new vertical diffusion package with an explicit treatment of entrainment processes. *Monthly Weather Review*, *134*(9), 2318–2341. https://doi.org/10.1175/MWR3199.1

Hu, X.-M., Nielsen-Gammon, J. W., & Zhang, F. (2010). Evaluation of Three Planetary Boundary Layer Schemes in the WRF Model. *Journal of Applied Meteorology and Climatology*, *49*, 1831–1844. https://doi.org/10.1175/2010JAMC2432.1

Jarosz, E., Mitchell, D. A., Wang, D. W., & Teague, W. J. (2007). Major Tropical Cyclone, *557*(March), 2005–2007.

Knabb, R. D., Rhome, J. R., & Brown, D. P. (2006). Tropical cyclone report: Hurricane Katrina, August 23-30, 2005. *Tropical Cyclone Report Hurricane Katrina*, 1–43.

Lacis, A., & Hansen, J. (1974). A parameterization for the absorption of solar radiation in the earth's atmosphere. *Journal of Atmospheric Sciences*, *31*(1), 118–133.

Mlawer, E. J., Taubman, S. J., Brown, P. D., Iacono, M. J., & Clough, S. A. (1997). Radiative transfer for inhomogeneous atmospheres: RRTM, a validated correlated-k model for the longwave. *Journal of Geophysical Research Atmospheres*, *102*(14), 16663–16682. https://doi.org/10.1029/97jd00237

Momen, M., Parlange, M. B., & Giometto, M. G. (2021). Scrambling and Reorientation of Classical Atmospheric Boundary Layer Turbulence in Hurricane Winds. *Geophysical Research Letters*, *48*(7). https://doi.org/10.1029/2020GL091695

Mooney, P. A., Mulligan, F. J., Bruyère, C. L., Parker, C. L., & Gill, D. O. (2019). Investigating the performance of coupled WRF-ROMS simulations of Hurricane Irene (2011) in a regional climate modeling framework. *Atmospheric Research*, *215*(August 2018), 57–74. https://doi.org/10.1016/j.atmosres.2018.08.017

NCAR. (2019). User's Guides for the Advanced Research WRF (ARW) Modeling System, Version 4, (January), 456.

NCEP, & GDAS. (2015). FNL 0.25 Degree Global Tropospheric Analyses and Forecast Grids. *Research Data Archive at the National Center for Atmospheric Research; Computational and Information Systems Laboratory: Boulder, CO, USA*.

NCEP National Centers for Environmental Prediction/National Weather Service/NOAA/US Department of Commerce. (2000). NCEP FNL operational model global tropospheric analyses, continuing from July 1999. *Research Data Archive at the National Center for Atmospheric Research, Computational and Information Systems Laboratory*.

Nolan, D. S., Stern, D. P., & Zhang, J. A. (2009). Evaluation of Planetary Boundary Layer Parameterizations in Tropical Cyclones by Comparison of In Situ Observations and High-Resolution Simulations of Hurricane Isabel (2003). Part II : Inner-Core Boundary Layer and Eyewall Structure. *Monthly Weather Review*, (11), 3675–3698. https://doi.org/10.1175/2009MWR2786.1

Pasch, R. J., Penny, A. B., & Berg, R. (2019). Hurricane Maria. *National Hurricane Center Tropical Cyclone Report: Hurricane Maria*, 1–69. Retrieved from https://www.nhc.noaa.gov/data/tcr/AL152017_Maria.pdf

Powell, M. D., Vickery, P. J., & Reinhold, T. A. (2003). Reduced drag coefficient for high wind speeds in tropical cyclones. *Nature*, *422*(6929), 279–283. https://doi.org/10.1038/nature01481

Skamarock, W. C., Klemp, J. B., Dudhia, J., Gill, D. O., Zhiquan, L., Berner, J., et al. (2019). *A Description of the Advanced Research WRF Model Version 4*. *NCAR Technical Note NCAR/TN-475+STR*. Retrieved from http://library.ucar.edu/research/publish-technote

Soloviev, A. V., Lukas, R., Donelan, M. A., Haus, B. K., & Ginis, I. (2014). The air-sea interface and surface stress under tropical cyclones. *Scientific Reports*, *4*, 1–6. https://doi.org/10.1038/srep05306

Wei, W., Bruyère, C., Duda, M., Dudhia, J., Gill, D., Kavulich, M., et al. (2019). *WRF ARW version 4 modeling system user's guide*.

Wicker, L. J., & Skamarock, W. C. (2002). Time-splitting methods for elastic models using forward time schemes. *Monthly Weather Review*, *130*(8), 2088–2097. https://doi.org/10.1175/1520-0493(2002)130<2088:TSMFEM>2.0.CO;2

Zhang, J. A. (2010). Spectral characteristics of turbulence in the hurricane boundary layer over the ocean between the outer rain bands. *Quarterly Journal of the Royal Meteorological Society*, *136*(649), 918–926. https://doi.org/10.1002/qj.610